Korean J. Chem. Eng., 35(10), 1955-1968 (2018)
DOI: 10.1007/s11814-018-0112-y
pISSN: 0256-1115
eISSN: 1975-7220

REVIEW PAPER

A review and recent developments on strategies to improve the photocatalytic elimination of organic dye pollutants by BiOX (X=Cl, Br, I, F) nanostructures

Sonal Singh*,‡, Rishabh Sharma,‡, and Manika Khanuja***,†**

*Shaheed Rajguru College of Applied Sciences for Women, University of Delhi, New Delhi-110096, India
**Thin Film Laboratory, Department of Physics, Indian Institute of Technology, New Delhi-110016, India
***Centre for Nanoscience and Nanotechnology, Jamia Millia Islamia, New Delhi-110025, India
(*Received 3 May 2018 • accepted 24 June 2018*)

Abstract−The main environmental problems associated with water body pollution are typically those caused by the discharge of untreated effluents released by various industries. Wastewater from the textile dye industry is itself a large contributor and contains a huge number of complex components, a wide spectrum of organic pollutants with high concentration of biochemical oxygen demand (BOD)/chemical oxygen demand (COD) and other toxic elements. One of several potential techniques to degrade such reactive dyes before being discharged to water bodies is photocatalysis, and bismuth-based photocatalysts are rapidly gaining popularity in this direction. Bismuth oxyhalides, BiOX (X=Cl, Br, I, F), as a group of ternary compound semiconductors (V-VI-VII), have been explored extensively for their photocatalytic activity due to their unique crystal lattice with special layered structure in pure as well as modified form. With suitable band gap and band edge positions, which are a required condition for efficient water breakup and high photon absorption, BiOCl scores over other oxyhalides. Photocatalytic activity depends on many factors such as synthesis method, morphology, size, illumination type, dye choice among others. This paper gives a critical review on bismuth oxyhalides as a family on various aspects of modifications such as doping (with unique and interesting metals as well), morphology and synthesis parameters, polymer and carbon assisted composites in order to further enhance the photocatalytic efficiency in UV/visible region of solar spectrum.

Keywords: Bismuth Oxyhalides, Photocatalysis, Pollutant Degradation, Factors, Strategies

INTRODUCTION

Poor management of organic waste leading to water pollution and associated environmental challenges are twin issues of utmost importance that require our prime concern and attention. With 20 percent of all fresh water pollution being caused during textile treatment and dyeing, the global textile and clothing industry still remains the major contributor to water pollution in the 21st century [1]. Various effluents from textile mills contain elevated levels of biochemical oxygen demand (BOD)/chemical oxygen demand (COD) [2] and solid suspensions, which leads to depletion of dissolved oxygen causing an adverse effect on the aquatic photosynthesis process, resulting in imbalance of the ecological system [2,3]. The BOD and COD ratio between 1 : 2 and 1 : 3 is generally acceptable and implies easy degradability of the wastes [4]. With increased pollutants and rising global consumption of fresh water doubling every 20 years, the population that is allergic to chemicals will reach 60% by the year 2020 [5]. More than 85% of unwanted matter can be removed by various effluent treatment methods [6]. Photocatalysis can cause fast and complete degradation of organic compounds economically and efficiently by treating the effluents for reduction in COD, BOD and other dissolved salts levels in wastewater. For this purpose, a large number of photocatalysts, such as TiO_2, ZnO, WO_3, MgO, Fe_2O_3, $BiVO_4$, Bi_2O_3, have already been explored so far to name a few [7-16].

Amongst these, bismuth, precisely bismuth oxyhalides, have caught our attention to a great extent. It is versatile and is emerging as a leading candidate in this direction. It is an environmentally benign element and a large class of photocatalysts exists for bismuth-based materials, which makes it unique with rest of the photocatalysts. Its use is found in a growing number of applications, such as pharmaceuticals, pigments in the cosmetic industry, phosphor, magnetic materials, gas sensors and catalysts [17-21]. Despite being a post-transition metal, it acts as a semiconductor when deposited as sufficiently thin layers [22]. Therefore, nanoscale bismuth is applied to catalysis and when modified suitably gives enhanced photocatalytic results and improves the efficiency of the system. Favorable characteristics of bismuth salts such as advantages of a unique crystal structure, excellent optical and electronic properties, low toxicity and ease of synthesis, associated with low cost, make them attractive and practical catalysts [23,24]. Li et al. nicely explained the role of layered structure of BiOX in meeting the demand of photocatalysis [25]. Moreover, its loosely bound structure, indirect band transitions and intrinsic internal electric field assist the photogenerated electron-hole pair's separation and their charge transfer, which makes them excellent photocatalyst [26]. Besides many such advantages, BiOX tends to suffer from certain issues like unfa-

†To whom correspondence should be addressed.
E-mail: manikakhanuja@gmail.com
‡These authors have contributed equally to this work.

vorable band edge positions and low photostability, which could lead to the catalyst poisoning of the suspended phases [27,28]. Particularly, BiOF is a wide and direct bandgap material, which makes it active only in UV region, thus results in inefficient utilisation of solar spectrum and reducing the lifetime of free charge carriers. BiOX nanoparticles have a property to agglomerate; thus their dispersion in aqueous solution during photocatalysis becomes difficult and hampers its photocatalytic activity. In BIOX, shadowing effect exists in which light is scattered by the photocatalyst before being absorbed [28]. Overcoming these issues will lead BiOX towards a suitable photocatalyst.

1. Fundamental Properties

Bismuth oxyhalides are inorganic compounds of Bi that belong to the class of matlockite mineral group. As the atomic number of X in BiOX increases, the band gap decreases, with a sequence of BiOF>BiOCl>BiOBr>BiOI, which gives a reason for the increase of photoactivity in the order BiOF<BiOCl<BiOBr<BiOI [29,30] (Fig. 1). The BiOX series is reported to exhibit p-type conductivity, but some also report n-type behavior [30,31]. BiOX, except BiOF, exhibits indirect band gap nature. An indirect band gap is favorable for the separation of photo-generated electron-hole pairs, while

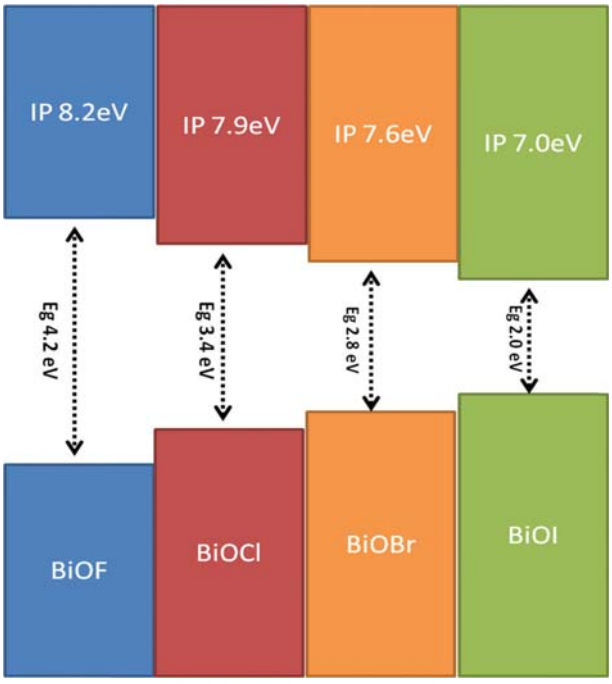

Fig. 1. Schematic illustrating band gap energy and alignment of BiOX series.

direct band gap is favorable for the absorption of photon energy [32]. BiOF and BiOCl are wide band gap materials with E_g greater than 3 eV. Band gap of BiOCl lies in the range 3.2-3.5 eV, which is almost similar to TiO_2 and thus provides a large scope of its improvement just like TiO_2. BiOI and BiOBr have suitable narrow band gaps of 1.8-1.9 and 2.6 eV, respectively, and thus have the ability to efficiently utilize the solar spectrum in visible light. BiOF, with widest band gap of 3.6 eV, does not show any visible light photoactivity, and thus only a few studies have reported on its photocatalytic activity (Table S4). Refer to Fig. S1 for absorption spectra for BiOX. However, in terms of UV-driven photocatalysis activity, it is still competitive with P25 [27]. Table 1 tabulates the fundamental properties of BiOX. Bi-X bonds are very long (>3 Å) except in the case of BiOF, which is around 2.78 Å. BiOCl and BiOBr have considerably smaller hole effective masses, m_h, than BiOF and BiOI as calculated by Ganose and groups using DFT calculations [33]. The values indicate an excellent mobility of electrons. The significant value difference between electron effective mass, m_e, and m_h indicates low recombination rate of e-h pairs, which means long lifetime and high diffusion rate of the carriers that are distinctly vital for augmenting photocatalytic activity [34].

2. Crystal Properties

The BiOX series are one of those few classes that exhibit layered structure type of arrangement. It exhibits tetragonal matlockite structure similar to PbFCl-type, with symmetry of P4/nmm (space group) and D 4 h (local symmetry) [35,36]. It is this peculiar arrangement of layered structure that helps them enormously to show high photoactivity. On crystallizing, bismuth oxyhalides acquire maklotite structure, which is one of the most simple forms of the Sillén-type structure [37]. A single bismuth layer is characterized by decahedral geometry where a Bi at center is surrounded by four atoms of oxygen and four atoms of halogens [25] (Fig. 2(a)). Such several single layers are stacked together by weak van der Waal forces through the halogen atoms along the c-axis but are bonded together by strong intralayer covalent bonding [38] as shown in Fig. 2(b). This anisotropic layered structure of BiOX, with interlayer and strong intralayer interactions, gives them a unique feature. They crystallize to form $[Bi_2O_2]^{2+}$ slabs interleaved by X^- ions (X=F, Cl, Br, I) with structure stacked together by interactions along the [001] direction to form [X-Bi-O-Bi-X] sheets [33].

The layered structure of pure and compounded bismuth oxyhalides has demonstrated outstanding photocatalytic activities. $[Bi_2O_2]^{2+}$ and X^- layers form an internal electric field between the layers which promotes and aids the separation of photoinduced electrons and holes pairs efficiently by polarizing the related atoms and orbitals between the layers, and therefore increasing their photo-

Table 1. Fundamental properties of BiOX series

Material	Band gap (eV)	CB (eV) [176]	VB (eV) [176]	Band gap type	Bond length (Å) [26]		Electron effective mass [33]		Lattice parameters
					Bi-O	Bi-X	Z→Γ	Z→R	
BiOCl	3.5	0.15	3.65	Indirect	2.3111	3.0424	0.3 m_e	2.4 m_e	a=b=3.8743 Å, c=7.3997 Å
BiOBr	2.6	0.41	3.01	Indirect	2.318	3.1648	0.3 m_e	0.6 m_e	a=b=3.8996 Å, c=8.4570 Å
BiOI	1.8	0.57	2.36	Indirect	2.3343	3.3515	--	--	a=b=3.9738 Å, c=9.3722 Å
BiOF	3.6	0.6	4.2	Direct	2.2769	2.7821	0.5 m_e	1.0 m_e	a=b=3.7386 Å, c=6.1714 Å

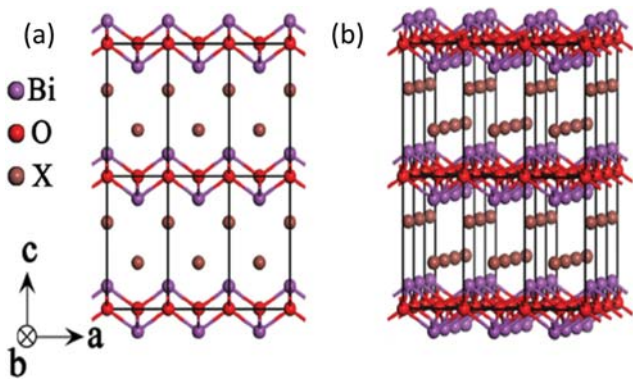

Fig. 2. (a) Unit cell, (b) supercell structure of BiOX (reproduced with permission of Zhao et al., Copyright 2014, American Chemical Society).

catalytic activity [27]. They not only demonstrate excellent photoactivity for NO oxidation, organic pollutant degradation and sterilization, but also show high adsorption ability for anionic organic dye through exchange of ions leading to release of X- and cationic dyes owing to the high density of terminated oxygen which are often found with negative {001} facet [39]. Sato group stated that the local internal fields due to the induced dipole moment help to promote the separation of charges in the very beginning of photoexcitation and are useful for improving photocatalytic activity [40].

3. Electronic Properties

Band dispersion diagram in Fig. 3(b), (c) and (d) for BiOCl, BiOBr and BiOI, respectively, shows that conduction band minimum (CBM) at Z point, while the valence band maxima (VBM) are positioned between Z-R making them indirect band gap materials. For BiOF, the both CBM and VBM are situated at Z, making it a direct band gap material as shown in Fig. 3(a) [41]. Previous theoretical literature studies of BiOX reveal that the VBM of BiOX catalysts is mainly composed of O 2p orbitals and X np states (X=F, Cl, Br and I and n=2, 3, 4 and 5, respectively). The CBM is mainly comprised of Bi 6p states. The contribution of X ns states increases with the increase in the X atomic number, which results in the decrease or narrowing of the bandgap value [42,43].

FACTORS AFFECTING PHOTOCATALYTIC ACTIVITY

1. Light Wavelength and Intensity

Change in photocatalytic properties of a material is strictly associated with the wavelength and intensity of light. Reports show that changing the energy of the incident photons could tune the photocatalytic reactions. This was indicated by Natarajan et al. where they demonstrated RhB dye degradation of BiOX samples using four types of light-emitting diodes (LEDs) with different wavelengths and exhibited different results [44]. It was observed that BiOCl and BiOBr almost completely degraded the dye under UVLED in 240 min as shown in Fig. 4I(a) and (b). This was mainly because the energy difference between VB and CB of synthesized samples matches with the range of irradiated light wavelength. Whereas, BiOI responded better to RLED irradiation with over 83.4% degradation of RhB dye and outperformed degradation under UVLED due to the magnificent production of holes or hydroxyl radicals under RLED (Fig. 4I(c)). Chang et al. used different wavelengths of visible light, with λ>400 nm, to decompose three different dyes of MO, MB, and RhB, which exhibited decomposition rates of 9.97%,

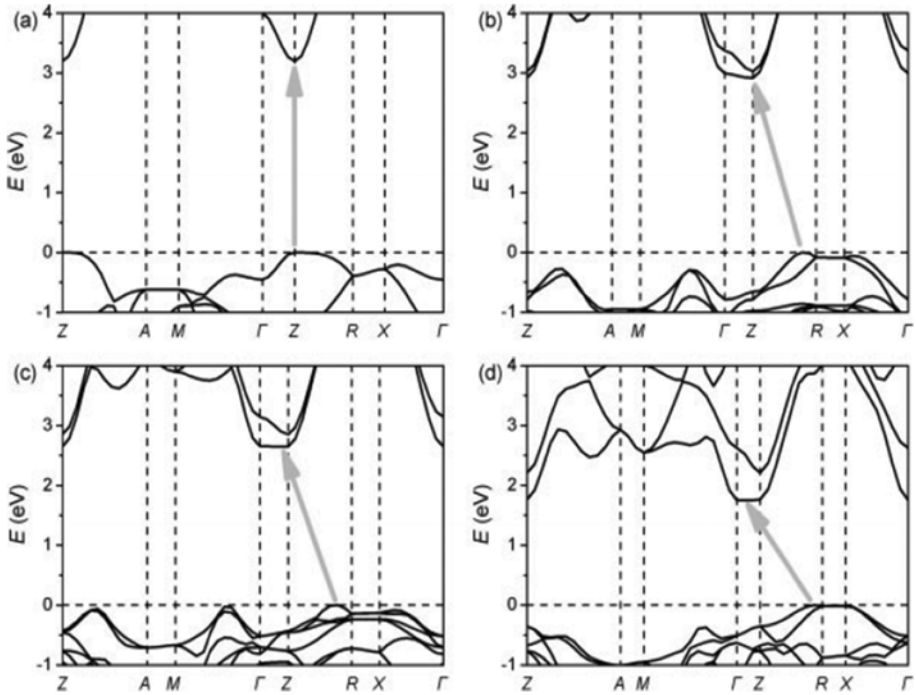

Fig. 3. Electronic band dispersion of BiOX series (a) BiOF, (b) BiOCl, (c) BiOBr, (d) BiOI (reproduced with permission of Huang et al., Copyright 2008, Wiley).

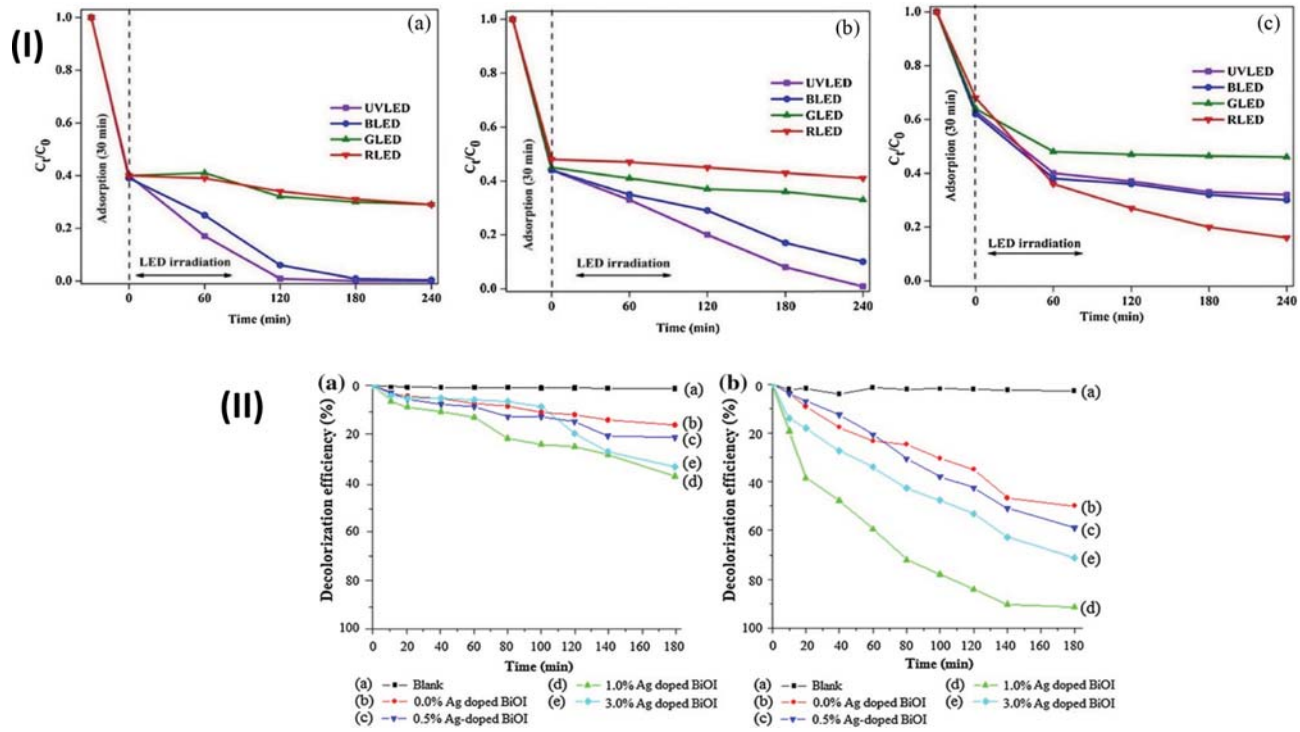

Fig. 4. (I) Effect of light wavelength on photodegradation of RhB under various LED irradiation (a) BiOCl, (b) BiOBr, (c) BiOI (reproduced with permission of Natarajan et al., Copyright 2016, Elsevier) and (II) effect of light intensity on decolorisation efficiency of MO aqueous solutions by BiOI under (a) UV light, and (b) daylight (reproduced with permission of Ekthammathat et al., Copyright 2015, Elsevier).

25.81% and 99.56%, respectively, in the presence of BiOBr. But when the wavelength was changed to λ>420 nm, the degradation of MB and MO with BiOBr was significantly reduced, but BiOBr still showed apparent degradation efficiency of 99.95% for RhB. Similarly, drastic results were found when BiOCl was studied under variable visible light irradiation wavelength. RhB removal efficiencies were found to be 94.91%, 99.50%, 53.76% under stimulation of λ>400 nm, λ>420 nm, and λ=550±15 nm, respectively, which clearly shows that amount of incident photons that contribute in photoreaction directly changes with incident wavelength (LED) [45].

Note that besides light wavelength, illumination intensity can affect the number of photogenerated electron-hole pairs produced and the efficiency of photo degradation of dye. As reported by Ekthammathat et al., the decolorization efficiency of Ag doped BiOI under sunlight was higher than that under UV lamp irradiation because the photonic energy or illumination intensity per second per surface area of the second light source is less than that of the first (Fig. 4II(a) and (b)) [46]. Other groups also illustrated the varying results in photocatalytic activity of BiOX (X=Cl, Br, I) on changing the illumination intensity [44,47].

2. Surface Area

It is known that the specific surface area of a material together with special porous structure is one factor that directly determines its photocatalytic activity, which in turn undoubtedly depends on the morphology of the material. These characteristics control the rate of release and utilization efficiency of .OH radicals. BET is an important technique used for the measurement and analysis of specific surface area. Many research groups have focussed on evaluating the influence on photocatalytic activity based on this aspect. Liu et al. reported that on increasing the doping concentration of Fe in BiOBr, the BET specific surface area was increased by formation of mesopores confirmed by type IV hysteresis loop, which enhances its photocatalytic activity [48] (Fig. S2). BiOCl/Carbon nanofiber heterostructures reported by Zhang et al. exhibited much higher removal efficiency for 4-nitrophenol than pure BiOCl [49]. Carbon nanofibers pose a large surface area, thus allowing the growth of dense and uniform growth of BiOCl nanosheets on its surface. Since BiOCl in this case is the active photocatalyst, so using CNF overall density of BiOCl is increased and hence photoactive surface area required for photoreactions is increased, thereby increasing the photocatalytic activity. As the size of the material shrinks, surface-to-volume ratio and number of surface dangling bonds increase drastically and enhance the chemical activity. A series of Ag-doped BiOI photocatalysts were developed by Ekthammathat et al. with different contents of metal doping [46]. It was noticed that with the increase of content of metal, morphology changed from nanoplates to agglomerated clusters, which reduced the surface area and thus had a negative effect on the photocatalytic activity of the sample. Microflower structured samples exhibited the best activity as they had the best exposure to aqueous solution owing to availability of large open surface area. Nanopores with bigger-pore-size allow multiple reflections of visible light within the interior and provide large photoactive surface area, thus enhancing the utilization and harvesting efficiency of visible light [50].

Table 2. Effect of $BiOI/TiO_2$ catalyst dosage on degradation rate of BPA removal [51]

Bi/Ti (molar rate)	Dose (g/L)	Initial pH	k_{obs} min^{-1}	R^2
25%	0.500	5.8	0.097	0.976
50%	0.500	5.8	0.150	0.987
75%	0.500	5.8	0.241	0.993
100%	0.500	5.8	0.039	0.971
75%	0.0	5.8	0.015	0.936
75%	0.33	5.8	0.122	0.998
75%	0.500	5.8	0.241	0.993
75%	0.667	5.8	0.234	0.987
75%	0.500	2.9	0.101	0.993
75%	0.500	5.0	0.146	0.985
75%	0.500	7.1	0.144	0.972
75%	0.500	9.0	0.222	0.997
75%	0.500	10.0	0.101	0.998

3. Catalyst Dosage

For effective degradation of any dye, the optimum amount of catalysts is an important parameter. It is generally observed that the degradation efficiency of a photocatalyst is increased with an increase in catalyst dosage up to a certain limit, but this efficiency starts decreasing after reaching a particular concentration. Liu and Chen group tested the photodegradation activity of BiOI-TiO_2 by varying the photo-catalyst dosage and keeping the dye concentration constant. For BiOI-TiO_2, the efficiency significantly enhanced for the range 0-0.500 g/L (Table 2) [51,52]. Similarly, Janani et al. studied the effect of increasing material loading from 0.1 to 0.8 g per 500 ml of MB dye solution with initial concentration of 50 mg/*l* and found a degradation percentage increase from 59.44 to 96.84%, respectively [53]. But further increase in catalyst dosage after achieving the optimized result led to a decrease in the degradation of the dye in all the cases. This may be explained on the basis of increased surface area with increase in material concentration, which in turn provides more adsorption and reaction sites as photocatalytic activity occurs on materials surface. Light scattering effect inhibits the production of hydroxyl and superoxide radicals and rejects the generation of electron and hole pair after increasing dosage above limiting value. Further, suspension turbidity and decreased light penetration may occur due to increased light scattering, which is the reason for low photocatalytic activity at higher concentration of catalyst.

4. Type of Dye and Dye Concentration

From the results of Liu and Chen group, it becomes very clear that when a material is tested for its photodegradation efficiency for different dyes but under similar conditions can lead to different results. Both the reports mention the preparation of x% BiOI/TiO_2 by same approach of microemulsion method for x% of 25, 50, 75 and 100. Samples presented almost similar morphology and tested under same light source of 250 W Halogen lamp for bisphenol A and methyl orange (Fig. 5(a) and (b)) [51,52]. Though both claimed to achieve maximum efficiency for x=75% sample but with different efficiency of 92 and 82.5%, respectively, which shows that different dyes may give different results. Values obtained for other x% samples also varied.

Along with choice of dye, it is very essential to choose the optimum concentration of dye. It was observed that the degradation rate was reduced with increase in the concentration of dye [44]. Maximum absorption of photons is a very necessary criterion for enhanced photocatalytic activity. But when the dye solution concentration increases, the photons get intercepted and consequently only fewer photons reach the surface of catalyst, resulting in less absorption, less .OH and O_2^- radicals and reduction in degradation percentage [54,55].

5. pH Value

PH value is another parameter that influences the availability of active sites on the surface of semiconductors, which affects the hydrogen ion or hydroxide ion concentration in aqueous solution [56]. Many studies have investigated the effect of pH value and concluded that generally reaction at neutral pH results in best deg-

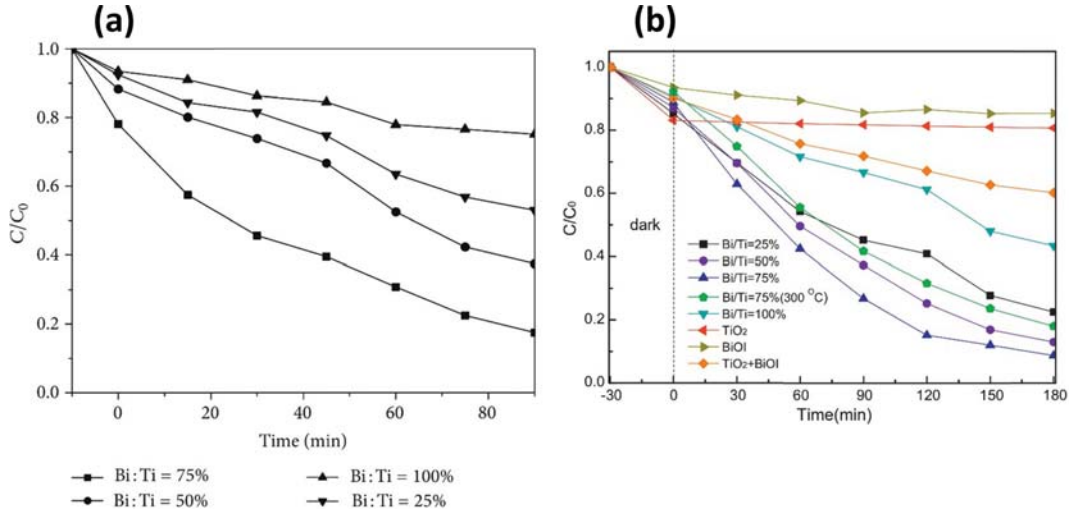

Fig. 5. Effect of different dye on $BiOI/TiO_2$ composite prepared under similar conditions on degradation of (a) BPA [51], (b) MO (reproduced with permission of Liu et al., Copyright 2012, Elsevier).

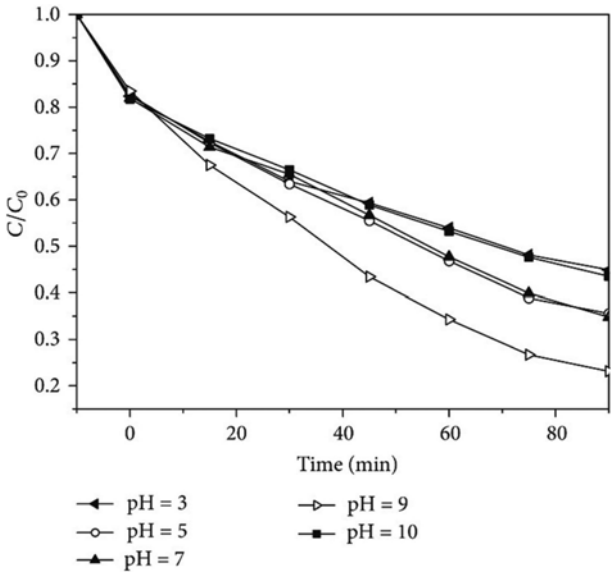

Fig. 6. Effect of pH on BPA removal rate of BiOI/TiO_2 catalysts dosage=0.5 g/L, BPA concentration=20 mg/L [51].

radation rates, while low photo-activity is recorded in high alkaline and acidic conditions. It is known that acidic condition inhibits the generation of OH radical and decreases the photocatalytic activity [57,58]. The RhB degradation efficiency of BiOI at pH=7, 2 and 4 was found to be 83.4, 70 and 61%. With the decrease in pH to 2 and 4, the degradation of RhB dye is reduced slightly, which was ascribed to the hydroxyl ions scavenging of by H^+ ions, which results in the decrease of degradation rate of RhB for this case [52]. Chen et al. also investigated the effect of pH on photocatalytic efficiency of BiOI/TiO_2 composite as shown in Fig. 6 [51]. They reported that in an acidic medium the photocatalytic dye degradation was reduced due to the same reason as reported above. Best photocatalytic activity was achieved at pH 9, i.e., alkaline medium. At pH 10, again the photocatalytic efficiency starts reducing. Point of zero charge (pzc) of a semiconductor is a deciding factor for protonation and deprotonation of photocatalyst surface at particular pH.

pH<pzc: $NOH+H^+=NOH_2^+$

pH>pzc: $NOH+OH^-=NOH^-+H_2O$

pH<pzc results in positively charged surface, while pH>pzc results in negatively charged surface of photocatalyst. Positively charged surface reduces the rate of hydroxyl ion generation (OH^-) which are responsible for dye degradation [59].

6. Natural Organic Matter and Carbonates

It has been previously reported that the presence of carbonate like Na_2Co_3 is beneficial for the photocatalysis process [60-63]. Infrared studies have revealed that the presence of carbonate salt in a solution results in absorption of carbonate species such as HCO_3^-, $CO_3^{\bullet-}$, $HCO_3^{\bullet}$, $C_2O_6^{2-}$ on the photocatalyst surface. These species are formed by gaining photogenerated holes and act as a hole scavenger. This scavenging of holes results in increased lifetime of free photoexcited electrons, which aids in enhancing photocatalytic performance. Although, this mechanism is still not well understood, but the results of photocatalytic performance with carbonates are outstanding [61].

Water collected from natural sources for photocatalytic purification always contains natural organic matter (NOM). NOM has an inhibitory effect on photocatalytic performance [64]. NOM gets adsorbed on the surface of photocatalyst and acts as a hydroxyl radical scavenger, thus reducing the photocatalytic performance. Reduction in photocatalytic performance depends on type of photocatalyst material; for example, TiO_2 has property to adsorb more NOM so the inhibitory effect of NOM on photocatalytic performance of TiO_2 is more pronounced. This could provide a great scope of exploration for researchers in case of BiOX which is still scant in this area.

7. Electronic and Structural Properties

As discussed in the introduction section, the electronic and structural properties of BiOX such as its unique layered crystal structure and nature of charge transition, i.e. direct or indirect, are important factors to decide their photoactivity. Indirect band gap offers an advantage of increasing the life time of free charge carriers by increasing their transition time. Thus more charge carriers are available for photoreactions in an indirect band gap material than a direct band gap material [14]. These factors have been well utilized as strategies to improve their photocatalytic activity, which are well established in many previous studies and are discussed in depth in next sections.

STRATEGIES TO IMPROVE PHOTOCATALYTIC EFFICIENCY IN BIOX

There exist several ways by which photoactivity of a material can be augmented. Charge carrier separation, large surface-to-volume ratio and light utilization efficiency remain the basic necessity for any enhanced performance. This can be achieved in numerous ways which are analyzed below (Various photocatalytic studies conducted on BiOX/modified BiOX are tabulated in supplementary information in Tables S1-S5.).

1. Doping

1-1. Metal Dopants

Various doping elements such as Ag, Fe, Ni, Ti, Al, Sn, In (Table S1-S3) have been used to form systems like Ag doped BiOI, Ti/Fe doped BiOBr, Fe/Ag/Ni/V doped BiOCl [46,48,65-67] that play an indispensable role in influencing the physical/chemical properties of the catalyst material by introduction of a foreign element, resulting in change of the lattice structure arrangement of the material. Metal doping benefits the inhibition of the recombination of generated electron and hole pair, a major disadvantage in mechanism of photocatalysis which lowers the efficiency and leads to energy wasting. Dopants cause trapping of electrons and help in encountering the recombination problem [68] and thus increase charge separation efficiency, which greatly enhances the generation of active oxygen species and hydroxyl radicals in photocatalysis [59,69].

1-2. Non-metal Dopants

Ever since the initial literature on non-metal doped TiO_2 (Nitrogen-TiO_2) was reported by Asahi et al. [70], a new set of possibilities opened in this area by using large number of non-metals such as N, C, S, F, I to realize visible light BiOX responsive photocatalysts (Table S1-S4). Non-metal doping is of special interest as it

succeeds in preserving the inherent surface properties of the photocatalyst when done at the atomic level. Dopants do not form clusters within the surface, rather existing in the form of isolated atoms [71]. Furthermore, dopant states are generally distributed and located close to the VB maximum, making photo-generated holes oxidative enough for subsequent photo-reactions. Non-metal dopants passivate the defect bands created by monodoping and help in reducing the recombination rate [72,73]. Jiang et al. showed that doping of BiOBr with N/S, N-, S-doped BiOBr displays the lowest VB position with the maximum band edge energy at about 2.51 eV and indirect band gap (IBG) transition [74]. IBG semiconductors assist to obtain excellent photocatalytic activity, as it is known that excited electrons reach the conduction band by traversing through certain k-spaces, thus reducing the recombination probability of the photogenerated charge carriers [75,76].

1-3. Noble Metal Dopants

Modification using noble metals such as Ag, Au, Pt, Rh, Pd is another good way to accelerate the photo-mechanism in BiOX, although a substantial number of reports are still lacking in this regard. It has been reported that the separation of photogenerated electrons and holes can be greatly promoted in the presence of the noble metal [77]. Silver doping has been the most intensively studied amongst all the noble-metal dopants [67]. Ekthammathat et al. results indicated that different Ag doping rates in BiOI showed different morphologies of nanoplates and microflowers. Varying photocatalytic results were obtained owing to change in optical properties and open surface area [46]. Comparatively, a large number of reports are available on noble-metal based-BiOX nanocomposites than doping as mentioned in section 2.4.3.

1-4. Rare Earth Metal Dopants

Certain reports exist on successful fabrication of BiOX nanostructures with rare earth metals dopants such as lanthanum (La) and europium (Eu) [66,78] and prove that the rare earth metal-doped BiOX semiconductors show improved photocatalytic effi-

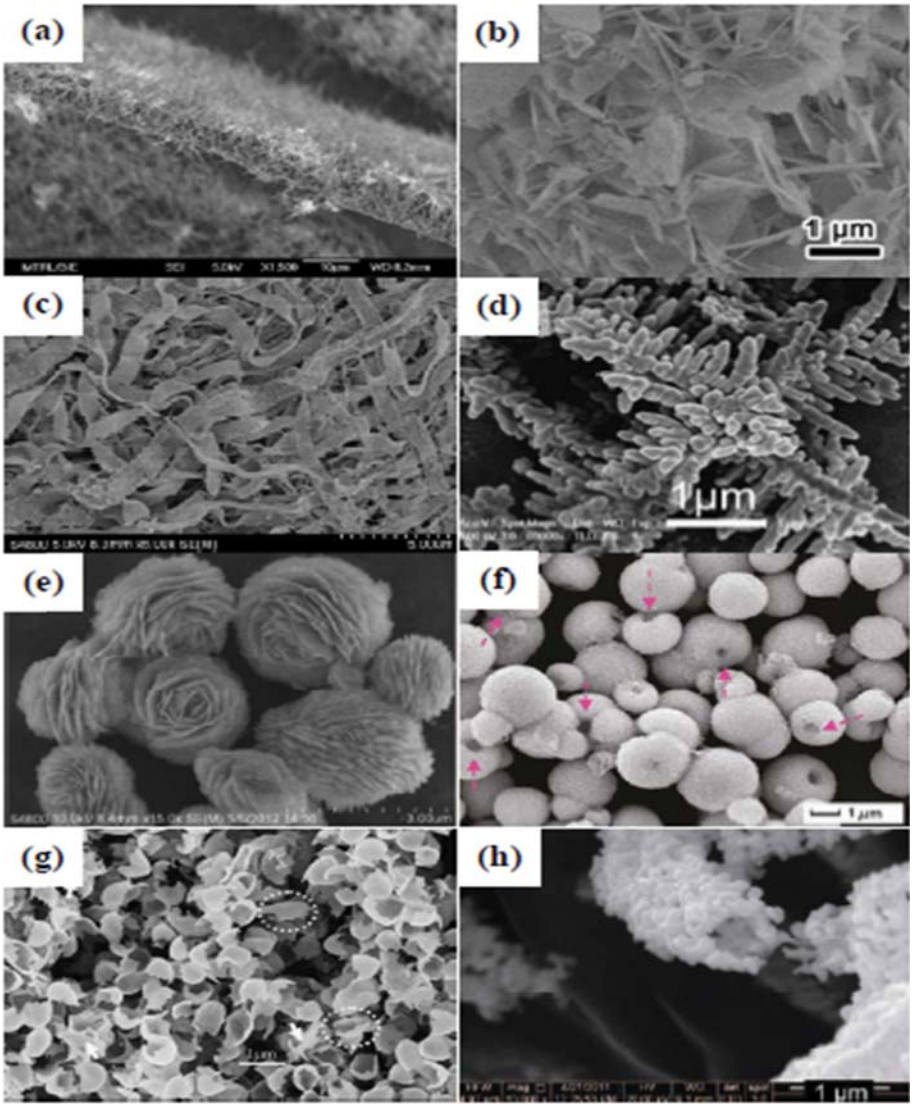

Fig. 7. Bi-based photocatalysts with different morphologies. (a) Nanowires, (b) nanoplates, (c) microbelts, (d) hyperbranches, (e) flower-like, (f) hollow microspheres, (g) eggshells, (h) hollowtubes (Reproduced with permission from He et al., Copyright 2014, Elsevier).

ciency (Table S1). Owing to their unique optical properties, rare earth elements with 4f electrons are broadly used as luminescent materials. They show magnificent response towards light either by direct utilization of excited electron in rare earth metal ion [79], or by indirect utilization of the emitted short wavelength light which are absorbed by semiconductors [80,81]. Dash et al. reported low temperature synthesis of Eu^{3+}-doped BiOX (X=Cl, Br, I) nanoflakes through microwave assisted green route and studied their optical, structural, and photocatalytic properties [82].

1-5. Bi-rich BiOX

Bismuth-rich technique is another viable way to augment the photocatalytic reduction activity for $Bi_xO_yX_z$ (X=Cl, Br, I). For instance, by bismuth-rich technique, $Bi_{24}O_{31}Br_{10}$ exhibited high photocatalytic activity for reduction of Cr(VI) and H_2 generation from water due to the upper shift in CBM position, leading to sufficient energy of electrons in CB to reduce O_2 to superoxide (O_2^-) [83]. In the process more free radicals are generated in bismuth rich $Bi_{24}O_{31}Br_{10}$. Also, in $Bi_4O_5Br_2$, bismuth-rich strategies and thickness-ultrathin result in remarkable photocatalytic reduction activity for CO_2 conversion due to change in the internal electrical filed of BiOX layers due to excess Bi [84]. Bai et al. for the first time displayed photocatalytic H_2 evolution for dominant {101} facets of bismuth-rich $Bi_4O_5X_2$ (X=Br, and I) nanosheets. $Bi_4O_5Br_2$ displayed efficient photocatalytic activity for H_2 production as compared to $Bi_4O_5I_2$ [85]. And more works like Bi_3O_4Br [86], Bi_3O_4Cl [87], Bi_5O_7I [88], Bi_5O_7Br [89] and $Bi_{24}O_{31}Cl_{10}$ [90] have proved that the bismuth-rich strategy can increase the photo response BiOX by displaying high photocatalytic activity for Cr (VI), CO_2 reduction and molecular oxygen.

2. Morphology and Facets

To date, a large number of Bi-based photocatalysts with well-ordered atomic structure composition and controlled morphology based arrangement of surface atoms have been explored to determine the photo-catalytic performance of nanocrystals (Fig. 7) [91]. Quantum size nanomaterials, with their length ranging from 1-100 nm in at least one dimension or more, such as 1-D (nanowires/belts/nanorods/fibers/tubes), 2-D (nanosheets/plates/films) or 3-D (flower-like, micro- and nanospheres, hour-glass like structure) are endowed with high surface-to-volume ratio, and thus more active sites with respect to their bulk counterparts, helps in better separation of photogenerated carriers produced during photocatalysis [92]. Nanoparticles with different shapes possess different facets and have different fraction of atoms located at different edges, corners and other defects resulting in difference of photocatalytic activity [93]. Synthesis technique, use of surfactants, polymers and other controlling agents widely impact the shape and morphology of the sample.

Pt-BiOBr composite with different morphologies of nanosheets, microflowers and microspheres exhibited different photocatalytic activity with spheres being 100% efficient in one hour [47]. Moreover, a crystal with different shapes can have different facets, which further decides the difference in photocatalytic activity of a material [93]. For example, Zhang et al. demonstrated that BiOCl nanosheets with {001} facets dominated the degradation of rhodamine B up to 94% in just 30 minutes and methyl orange up to 79% in 2 hrs under visible light [94]. After employing DFT calculations, Zhang and co-workers suggested that BiOBr with {102} exposed facet have superior photocatalytic activity as compared to {001} facet and also validated this experimentally. Due to surface states of {102} facets, they have higher VBM level (which results in more efficient electron injection), higher redox potential of hole and reduced band gap observed by red shift in the absorption [95]. Photocatalytic property of the {010}, {110}, and {001} facets within BiOXs has been compared by Zhang et al. [96] and found {001} facets to be more thermodynamically stable with efficient charge carrier separation due to fewer surface states and surface dangling bonds. However, facets with higher surface energies are usually more reactive than thermodynamically stable facets [97,98]. Further, the {001} facet-dependent improved photoactivity of BiOX (X=Cl, Br, I) single-crystal nanosheets has also been investigated [99-102]. Fig. 8 shows the schematic diagram of facet-dependent photo reactivity of BiOCl single-crystalline nanosheets.

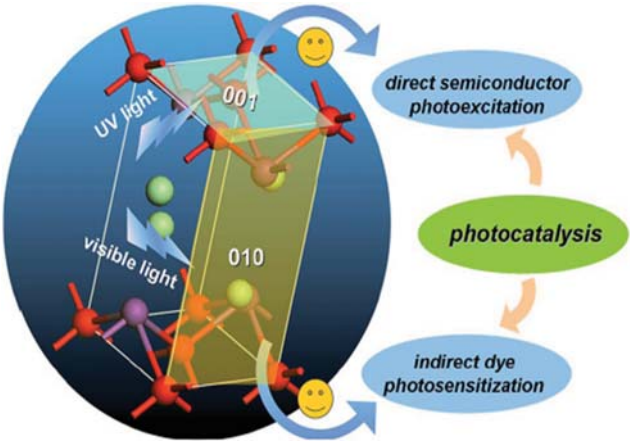

Fig. 8. Schematic diagram of facet-dependent photo reactivity of BiOCl single-crystalline nanosheets (Reproduced with permission from Jiang et al., Copyright 2012, ACS).

3. Synthesis Parameters

Engineering the morphology and its related characteristics like shape, size and dimensionality of the product paves a new way to enhance photocatalytic activity, which can be achieved by controlling the synthesis techniques and its parameters. By far, hydrolysis is the simplest synthesis method available for BiOX. On dispersing bismuth and halogen sources to the aqueous solution, Bi^{3+} cations tend to react with water to yield $(Bi_2O_2)^{2+}$ and H^+ cations initially, which slowly forms into innumerable tiny crystalline nuclei of X-Bi-O-Bi-X through coulomb coupling interactions between negative X^- anions and positive $(Bi_2O_2)^{2+}$ cations. 2D structure of [X-Bi-O-Bi-X] slices is favored by the aggregation of X-Bi-O-Bi-X along the direction perpendicular to the c-axis. Freshly formed slices stack together by weak van der Waal forces through the halogen atoms, when left for prolonged ripening [25]. However, shortcomings like poor dispersion and uncontrollable morphology are still associated with this method [27].

Also, hydrothermal and solvothermal are the most accepted and commonly used methods because of their simplicity, cleanliness and ease of convenience. But at the same time, they may prove disadvantageous due to the involvement of heat treatment, high pres-

sures, use of surfactants or additives and the need to dispose of residue solvents. Therefore, low temperature synthesis may be another simple and essential route for synthesis as demonstrated by Xie et al. for rapid and uniform production of BiOI's [103]. Microwave-assisted synthesis is sometimes preferred over conventional heating methods since microwaves promote transformations by directly transferring energy to the reactive species and completing the reaction in minutes. The process results in localized instantaneous superheating of the material that reacts to either ionic conduction or dipole rotation of energy transferring mechanism [104]. Simultaneously, it proves to be clean, simple, low energy consumption, low cost and environment friendly [82,105]. Synthesis parameters--temperature, time, molar concentration or weight percent ratios of materials in nanocomposites, use of controlling agents, solvent--also play a major role in deciding the shape and structure of a material (Table S1-S5). Liu et al. investigated the effects of hydrothermal reaction time and temperature on morphology, crystal orientation and photo-catalytic efficiency of the BiOI samples and obtained the best results at synthesis of 160 °C for 30 hours which could degrade RhB up to 88% in just 50 minutes over other combinations of temperature and time [106]. BiOCl tested for different concentrations of KBH_4 ranging from 0.01 M to 0.05 M in Bi_2O_3/BiOCl [107] or x wt% Bi_2O_3-BiOCl from 1 to 4 wt% [108] yielded different results of photoactivity. Use of polymer assisted synthesis has been demonstrated by use of polyethylene glycol 600 as solvent for BiOBr [109] and polyvinylpyrrolidone (PVP) for BiOCl [110,111] as a surfactant, which influences the formation of BiOCl into hierarchical nest-like and hollow structure. Concentration of PVP in the mixture can selectively attach and insulate the growth of the plane. In addition, it is used to manipulate the band gaps of material [112]. Guo et al. clearly showed that by adjusting solvents, such as absolute ethanol, water, 2-methoxyethanol or PVP and ethylene glycol, and Br sources during the synthesis, BiOBr crystals with different morphologies were fabricated and that the photocatalytic properties of the catalysts depend highly on the type of morphology [47].

4. Composite/Heterostructures

4-1. Composite with Carbon Material

Of late, many research groups have demonstrated the use of carbon materials to construct efficient photocatalytic composites/heterostructure to enhance the photocatalytic activity and electrochemical behavior of BiOX materials. Graphene (GR), already known for its superior properties such as high electron mobility, conductivity and extremely high specific surface area, proves a potential candidate in photocatalysis as evidenced from the reports. Tang et al. obtained a series of GR/BiOCl prepared by solvothermal method and found that BiOCl-30% GR showed the optimum activity towards visible light due to more effective charge separations and from the synergetic effect between GR and BiOCl [113]. 2D carbon material with single atomic layer, such as reduced graphene oxide (RGO), has zero band gap and with its unique electronic structure and is capable of absorbing light from UV and near-IR region. 2D π-conjugation structure of graphene makes it an excellent electron acceptor. For example, Wang et al. showed RGO (5 wt%)-(U)BiOCl composite resulted in increased degradation of rhodamine B under UV as well as visible light as compared to bare BiOCl of similar sized particles. The fast degradation of 96% RhB in 3.5 min was attributed to increased light absorption, which then resulted in effective charge transportation and faster interfacial charge-transfer process [114]. Kang et al. also demonstrated that size-controlled BiOCl-RGO composites degraded RhB completely in 310 min, which was due to high surface area of composite and reduced recombination losses [115].

1D carbon materials, such as carbon nanotube (CNT) and carbon nanofiber (CNF) have also proved their potential in photocatalysis. Since CNTs' were first used to improve the photon adsorption of TiO_2 [116,117], plenty of literature exists to develop heterojunctions using 1D material. They provide the advantage of (1) efficiently capturing and transporting photogenerated electrons through highly conductive long 1D nanostructures, (2) large surface areas and open structures of fibers/tubes provide more active sites for capturing BiOX nanostructures with both good dispersion and high density, and (3) The nanofibers possesses nanofibrous nonwoven structures which renders them with favorable recycling characteristics, and thus can easily be separated from solution by sedimentation without a reduction in photocatalytic activity [49,118].

0D nanocarbon quantum dots (CQDs) exhibit unique chemical, physical and photoelectrochemical properties such as high aqueous solubility, low cytotoxicity, excellent photoluminescence (PL), excellent biocompatibility and superior chemical stability. Use of CQDs with usually wide band gap semiconductors, such as BiOCl, makes them efficient photocatalyst due to their superior properties, such as large absorption coefficients, broad absorption spectrum, outstanding photo induced electron transfer and electron reservoir [119]. Coupling of CQDs with BiOX has been reported by many research groups [120-122].

Another important carbon material, C_3N_4, has also been composited with BiOCl, BiOBr and BiOI due to its high nitrogen content, which can provide more active sites. Bai et al. showed an enhanced RhB degradation of BiOCl-gC_3N_4 photocatalyst via direct Z-scheme, enabling the photoinduced charge transfer between the CB of BiOCl and the VB of gC_3N_4 [123]. Even Ag-doped BiOF exhibited improved photocatalytic performance when coupled with C_3N_4 [124] (Table S4).

4-2. Semiconductor/BiOX and BiOX/BiOY Heterostructures (X, Y=Cl, Br, I; X≠Y)

When a heterojunction is formed between semiconductors of matching band gap energies, photogenerated charge carriers can be transported from one semiconductor to other through contact potential, thus reducing the recombination rate of photogenerated electron-hole pair**.** Mehraj et al. [125] studied the photocatalytic activity of Ag_3PO_4/BiOBr heterojunction. Due to the band edge position of two semiconductors, photoexcited electrons in CB of Ag_3PO_4 hop to CB of BiOBr and holes from VB of BiOBr hop to VB of Ag_3PO_4 thereby increasing the efficiency of charge separation and enhancing photocatalytic activity. BiOI/TiO_2, $BiPO_4$/BiOI, BiOBr/$ZnFe_2O_4$, WO_3/BiOCl, Bi_2MoO_6/BiOCl [126-130] are few examples of BiOX/semiconductor heterojunction.

Reports show that BiOX/BiOY show higher photocatalytic activity as compared to BiOX alone, as this structure leads to the generation of more photoexcited electron-hole pairs [131-133]. Liu et al. prepared BiOI/BiOBr heterostructure films and found an in-

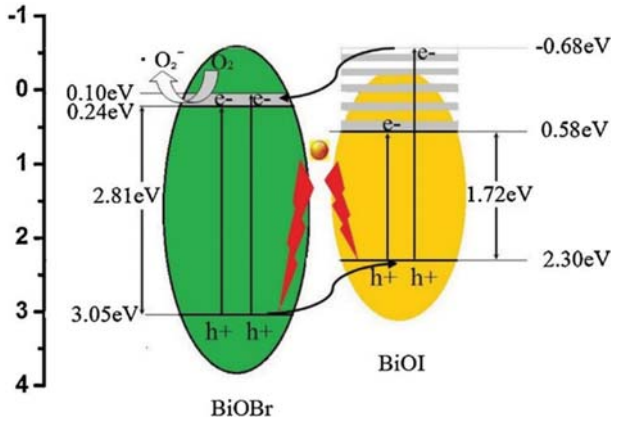

Fig. 9. Schematic band structure of BiOI/BiOBr heterostructure film (Reproduced with permission from Liu et al., Copyright 2014, Elsevier).

creased dye degradation of methyl orange (MO) under visible light compared to pure BiOBr film. It showed highest activity due to suitable band gap energies, high specific surface, and the low recombination rate of the photogenerated electron-hole pairs [134]. They calculated the band edge potentials using Mulliken electronegativity theorem and showed the charge transfer through the heterojunction from BiOI CB to BiOBr CB. This charge transfer through heterojunction results in reduction in the recombination of the charge carriers and also low band gap of BiOI is acting as a light sensitizer, thus improving the overall photocatalytic performance of this heterojunction. Band diagram of the heterojunction is shown in Fig. 9. Similar results were achieved by Jiang et al. for the series of BiOI/BiOBr. The photocatalytic activity was found to be 10 times higher than that of P25-TiO_2, 6 times higher than BiOI and 14 times higher than BiOBr [135]. Other heterojunction examples include BiOCl/BiOBr, BiOI/BiOCl, BiOCl/$BiVO_4$, BiOCl/C_3N_4 [27,133, 136,137] (Table S5).

4-3. Noble Metal Composites

Of late, noble metal-modified semiconductors nanostructures have become the focus of study with Ag, Rh, Pd, Pt-Ag being the most exploited noble metals [138-140]. The effects of noble metal deposition (Rh, Pd, Pt) to prepare Noble metal/BiOX (Cl, Br, I) composite photocatalysts on the photocatalytic performance and optical properties of BiOX in degradation of the acid orange II dye under both visible light and UV irradiation were systematically investigated [141]. Concentration and species of noble metal controls the overall enhanced performance of photocatalytic activity. When tested for BiOCl, the photoactivity under UV light and visible light irradiation was found in the order of Pt>Pd>Rh and Rh>Pt>Pd, respectively. Over other BiOX, it followed the sequence Pd(0.5%)/BiOBr>Pt(1%)/BiOCl>Pd(2%)/BiOCl under UV, while it changed to Pd(4%)/BiOBr>Pd(0.5%)/BiOI>Rh(1%)/BiOCl under visible light illumination. The enhanced performance was attributed to increased charge separation and plasmonic effects caused by noble metal nanoparticles.

4-3-1. Surface Plasmon Resonance (SPR) Effect

Much advancement has also been seen in photocatalytic properties of noble material-based composites involving the surface plasmon resonance effect. Among the noble metals, Ag shows the best SPR activity. A majority of publications discuss the coupling of strong plasmonic nanoparticles to enhance the net activity of the photocatalytic processes, such as Ag/AgX (X=Cl, Br, I), Ag-TiO_2, Ag/AgBr, Ag-ZnO, Ag/AgBr/TiO_2, Ag/$AgPO_4$, Ag/AgBr/Bi_2WO_6, and Ag/AgBr/WO_3 [142-152], as these noble nanoparticles absorb light in visible region via SPR. Similar attempt has been made in designing Ag/BiOX or Ag/AgX/BiOX systems (Fig. 5) [153-159]. In surface plasmon resonance, whenever light stimulates the surface of the conducting material, free charges produce oscillations confined to the material's surface. When the value of dielectric function approaches to zero, the resonance in absorption can be seen at this particular plasmon frequency. This frequency of resonance can be controlled or changed by making some changes in size or shape of the nanoparticles [159-163]. For example, by tuning the size of nanoparticles, the plasmon resonance can be shifted from UV to visible region, and from visible to infrared wavelength range in case of Ag and Au, respectively. Photocatalytic activity of a material can be increased by storage of electrons in co-catalyst metal nanoparticles through SPR, and that leads to decrease in charge recombination. Storage of electrons in metal nanoparticles is detected by blue shift in SPR frequency, which leads to a shift in Fermi level towards negative potential [164,165].

4-4. Polymer Composites

Some efforts have also been made to modify the materials with polymer-assisted approach. Conjugated polymers with extended π-conjugated electron systems show tremendous absorption region in the visible light range, excellent stability and high mobility of charge carriers [166]. Polymers like polypyrrole, polyaniline, polythiophene and their derivatives are commonly used to assist the reaction. Additionally, PANI as conducting polymer is relatively easy to synthesize and cheap when compared with doped noble metals [167]. Though much work has been demonstrated on photocatalytic activity by constructing heterogeneous conducting polymer composite specially for TiO_2 [168-170] and other materials, it still provides considerable scope for BiOX which is still quite naïve [110,112,171].

5. Synergistic Coupling Effect

Synergistic effects arise when something x is 'united with' y. In simple terms, it is an effect that arises between two or more entities, agents, or substances that produces an effect greater than the sum of their individual effects. It means to unite a material with another sub material to accomplish desired results which could not be achieved by either material alone. Such a heterogeneous synergistic reaction has much significance in the degradation mechanism of organic pollutants in conventional photocatalysis reaction.

Nussbaum et al. found that BiOCl, when co-doped with iron and niobium, the dye was degraded by strong synergistic effect [66] (Fig. 6). This synergistic effect was introduced by local interactions between co-dopant (Fe and Nb) and dye molecules rather than high crystallinity or change in optical properties of the BiOCl. It is known that Fe ions have tendency to form complexes with rhodamine [172]. Dye molecules have specific interaction with metal atoms existing on the surface of the BiOCl matrix. Although this did not hold valid in the case of BiOCl when doped with Fe only, which resulted in the formation of particular phase of Fe_2O_3 on the sur-

face, thus inactivating complex formation with the Rhodamine, unlike Fe^{3+} in BiOCl (Fe, Nb) and thus showed poor photocatalytic activity. Similarly, it was observed in PANI/BiOCl photocatalysts where BiOCl alone could not be excited under visible light but coupling with PANI caused synergistic effect by inducing π-π* transition. Under this condition, significantly enhanced photocatalytic activity was achieved by delivering the excited-state electrons of HOMO orbital to LUMO orbital, which yields superoxide and hydroxyl radicals on reacting with oxygen and water and thus oxidises the dye [167].

6. Dye Sensitization

Another facile approach for the enhancement of photocatalysis is by means of dye sensitization.

Under visible light irradiation, the excited dyes can initiate catalytic reactions by injecting electrons to CB of semiconductors. It is a very effective method to extend the spectrum to the visible range as is reported in the literature. For instance, Yu et al. demonstrated dye sensitized photocatalytic activity of $Bi_2O_2CO_3$/BiOCl and found that it is even more photoactive under visible light than P25 under UV light for RhB degradation. The increase of H_2O_2 was attributed to the photosensitization of RhB, which makes the photocatalytic degradation go smoothly [173]. Mao et al. also explained the role of RhB as a photosensitizer that can remarkably improve utilization of light and increase the photocatalytic activity of BiOCl for degradation of bisphenol-A [174]. Li et al. developed an extremely efficient BiOCl-RhB system with strong adsorption of RhB on BiOCl spheres on the exposed {001} facets that acts as an electron transfer channel from BiOCl to RhB and thus aids in the reduction of RhB more efficiently [175].

CONCLUSION

Parameters like unique layered crystal structure and photo stability of bismuth oxyhalides based nanomaterials have gained considerable popularity worldwide for their contribution in the field of photocatalysis and water splitting applications. Emphasis has been laid on adopting various ways of tailoring and altering their optical properties that are responsible for making them highly photo responsive by providing more surface area and more photoactive sites for reactions to take place. Unlike BiOF, which comparatively suffers fast recombination rate of charge carriers and thus has poor performance in this field of application, BiOCl, BiOBr and BiOI exhibit improved charge separation performance due to appropriate band gap energies and indirect band alignment. New plasmonic materials with low cost and better performance will be needed in the long run for industrial applications. However, the use of noble metals as co-catalyst to modify BiOX may raise the cost of production as they are rare and expensive. Other earth abundant metals that are relatively affordable and economical such as Ni and Al, and fascinating carbon-based materials such as GO, RGO, quantum dot need to be explored at a large scale to be widely accepted in this application. With TiO_2 and ZnO as commercially used photocatalysts, BiOX is still at a naïve state, which opens a new set of possibilities and offers much scope for further improvement. With promising results so far, we hope our attempt to review the development of visible light driven effectual BiOX photocatalyst will have an impact on people working in this area of energy and environment.

ACKNOWLEDGEMENTS

The authors wish to acknowledge Industrial Research and Development (IRD), Indian Institute of Technology (IIT), Delhi, India for providing all necessary facilities during this study work.

SUPPORTING INFORMATION

Additional information as noted in the text. This information is available via the Internet at http://www.springer.com/chemistry/journal/11814.

REFERENCES

1. T. Robinson, G. McMullan, R. Marchant and P. Nigam, *Bioresour. Technol.*, **77**, 247 (2001).
2. A. Ashfaq and A. Khatoon, *Int. J. Curr. Microbiol. Appl. Sci.*, **3**, 780 (2014).
3. J. C. Davis, *J. Fish. Board Canada*, **32**, 2295 (1975).
4. R. Chavan, *Indian J. Fibre Text. Res.*, **26**, 11 (2001).
5. R. Kant, *Nat. Sci.*, **4**, 22 (2012).
6. G. Tchobanoglous and F. L. Burton, *Management*, **7**, 1 (1991).
7. G. Xi, B. Yue, J. Cao and J. Ye, *Chem. Eur. J.*, **17**, 5145 (2011).
8. K. Vinodgopal and P. V Kamat, *Environ. Sci. Technol.*, **29**, 841 (1995).
9. M. Niu, F. Huang, L. Cui, P. Huang, Y. Yu and Y. Wang, *ACS Nano*, **4**, 681 (2010).
10. E.-J. Li, K. Xia, S.-F. Yin, W.-L. Dai, S.-L. Luo and C.-T. Au, *Mater. Chem. Phys.*, **125**, 236 (2011).
11. S. Singh, R. Sharma, G. Joshi and J. K. Pandey, *Korean J. Chem. Eng.*, **34**, 500 (2017).
12. R. Sharma, M. Khanuja, S. S. Islam, U. Singhal and A. Varma, *Res. Chem. Intermed.*, **43**, 5345 (2017).
13. S. Singh, R. Pendurthi, M. Khanuja, S. S. Islam, S. Rajput and S. M. Shivaprasad, *Appl. Phys. A*, **123**, 184 (2017).
14. R. Sharma, M. Khanuja, S. N. Sharma and O. P. Sinha, *Int. J. Hydrogen Energy*, **42**, 20638 (2017).
15. S. Singh, R. Sharma and B. R. Mehta, *Appl. Surf. Sci.*, **411**, 321 (2017).
16. R. Sharma, Uma, S. Singh, A. Verma and M. Khanuja, *J. Photochem. Photobiol. B Biol.*, **162**, 266 (2016).
17. G. Auer, W. D. Griebler, B. Jahn, G. Buxbaum and G. Pfaff, Wiley-VCH Verlag GmbH Co. KGaA, Weinheim, 129 (2005).
18. G. G. Briand and N. Burford, *Chem. Rev.*, **99**, 2601 (1999).
19. R. Ghosh, S. Maiti and A. Chakraborty, *Tetrahedron Lett.*, **45**, 6775 (2004).
20. C. R. Michel, N. L. L. Contreras and A. H. Martínez-Preciado, *Sensors Actuators B Chem.*, **160**, 271 (2011).
21. J. G. Rabatin, U.S. Patent 4,068,129 (1978).
22. C. A. Hoffman, J. R. Meyer, F. J. Bartoli, A. Di Venere, X. J. Yi, C. L. Hou, H. C. Wang, J. B. Ketterson and G. K. Wong, *Phys. Rev. B*, **48**, 11431 (1993).
23. R. Hua, *Curr. Org. Synth.*, **5**, 1 (2008).

24. T. Ollevier, *Org. Biomol. Chem.*, **11**, 2740 (2013).
25. J. Li, Y. Yu and L. Zhang, *Nanoscale*, **6**, 8473 (2014).
26. Z.-Y. Zhao and W.-W. Dai, *Inorg. Chem.*, **53**, 13001 (2014).
27. Z. He, Y. Shi, C. Gao, L. Wen, J. Chen and S. Song, *J. Phys. Chem. C*, **118**, 389 (2014).
28. F. Shen, L. Zhou, J. Shi, M. Xing and J. Zhang, *RSC Adv.*, **5**, 4918 (2015).
29. P. Wei, Q. Yang and L. Guo, *Prog. Chem.*, **21**, 1734 (2009).
30. H. F. Cheng, B. B. Huang and Y. Dai, *Nanoscale*, **6**, 2009 (2014).
31. N. T. Hahn, S. Hoang, J. L. Self and C. B. Mullins, *ACS Nano*, **6**, 7712 (2012).
32. Z.-Y. Zhao and W.-W. Dai, *Inorg. Chem.*, **54**, 10732 (2015).
33. A. M. Ganose, M. Cuff, K. T. Butler, A. Walsh and D. O. Scanlon, *Chem. Mater.*, **28**, 1980 (2016).
34. X. Zhang, B. Li, J. Wang, Y. Yuan, Q. Zhang, Z. Gao, L.-M. Liu and L. Chen, *Phys. Chem. Chem. Phys.*, **16**, 25854 (2014).
35. F. A. Bannister, *J. Mineral. Soc.*, **24**, 49 (1935).
36. K. G. Keramidas, G. P. Voutsas and P. I. Rentzeperis, *Zeitschrift Fur Krist. - New Cryst. Struct.*, **205**, 35 (1993).
37. A. M. Kusainova, W. Zhou, J. T. S. Irvine and P. Lightfoot, *J. Solid State Chem.*, **166**, 148 (2002).
38. K.-L. Zhang, C.-M. Liu, F.-Q. Huang, C. Zheng and W.-D. Wang, *Appl. Catal., B Environ.*, **68**, 125 (2006).
39. H. Zhao, F. Tian, R. Wang and R. Chen, *Rev. Adv. Sci. Eng.*, **3**, 3 (2014).
40. J. Sato, H. Kobayashi and Y. Inoue, *J. Phys. Chem. B*, **107**, 7970 (2003).
41. W. L. Huang, *J. Comput. Chem.*, **30**, 1882 (2009).
42. D. S. Bhachu, S. J. A. Moniz, S. Sathasivam, D. O. Scanlon, A. Walsh, S. M. Bawaked, M. Mokhtar, A. Y. Obaid, I. P. Parkin and J. Tang, *Chem. Sci.*, **7**, 4832 (2016).
43. W. L. Huang and Q. Zhu, *Comput. Mater. Sci.*, **43**, 1101 (2008).
44. K. Natarajan, H. C. Bajaj and R. J. Tayade, *J. Ind. Eng. Chem.*, **34**, 146 (2016).
45. X. Chang, M. A. Gondal, A. A. Al-Saadi, M. A. Ali, H. Shen, Q. Zhou, J. Zhang, M. Du, Y. Liu and G. Ji, *J. Colloid Interface Sci.*, **377**, 291 (2012).
46. N. Ekthammathat, S. Kidarn, A. Phuruangrat, S. Thongtem and T. Thongtem, *Res. Chem. Intermed.*, **42**, 5559 (2015).
47. W. Guo, Q. Qin, L. Geng, D. Wang, Y. Guo and Y. Yang, *J. Hazard. Mater.*, **308**, 374 (2016).
48. Z. Liu, B. Wu, Y. Zhu, D. Yin and L. Wang, *Catal. Lett.*, **142**, 1489 (2012).
49. M. Zhang, C. Shao, X. Zhang and Y. Liu, *CrystEngComm*, **17**, 7276 (2015).
50. W. Cai, G. Duan and Y. Li, Hierarchical Micro/Nanostructured Materials: Fabrication, Properties, and Applications, CRC Press (2014).
51. Y. Chen, X. Xu, J. Fang, G. Zhou, Z. Liu, S. Wu, W. Xu, J. Chu and X. Zhu, *Sci. World J.*, **2014** (2014).
52. Z. Liu, X. Xu, J. Fang, X. Zhu, J. Chu and B. Li, *Appl. Surf. Sci.*, **258**, 3771 (2012).
53. S. Janani, S. R. KS, P. Ellappan and L. R. Miranda, *J. Environ. Chem. Eng.*, **4**, 534 (2016).
54. M. A. Behnajady, N. Modirshahla and R. Hamzavi, *J. Hazard. Mater.*, **133**, 226 (2006).
55. C. C. Chen, C. S. Lu, Y. C. Chung and J. L. Jan, *J. Hazard. Mater.*, **141**, 520 (2007).
56. C. Wang, H. Zhang, F. Li and L. Zhu, *Environ. Sci. Technol.*, **44**, 6843 (2010).
57. H.-S. Son, S.-J. Lee, I.-H. Cho and K.-D. Zoh, *Chemosphere*, **57**, 309 (2004).
58. H.-S. Son, G. Ko and K.-D. Zoh, *J. Hazard. Mater.*, **166**, 954 (2009).
59. K. M. Lee, C. W. Lai, K. S. Ngai and J. C. Juan, *Water Res.*, **88**, 428 (2016).
60. K. Sayama and H. Arakawa, *J. Photochem. Photobiol. A Chem.*, **77**, 243 (1994).
61. K. Sayama and H. Arakawa, *J. Photochem. Photobiol. A Chem.*, **94**, 67 (1996).
62. K. Sayama, H. Arakawa and K. Domen, *Catal. Today*, **28**, 175 (1996).
63. K. Sayama and H. Arakawa, *J. Chem. Soc. Chem. Commun.*, **2**, 150 (1992).
64. J. Brame, M. Long, Q. Li and P. Alvarez, *Water Res.*, **84**, 362 (2015).
65. R. Wang, G. Jiang, X. Wang, R. Hu, X. Xi, S. Bao, Y. Zhou, T. Tong, S. Wang, T. Wang and W. Chen, *Powder Technol.*, **228**, 258 (2012).
66. M. Nussbaum, N. Shaham-Waldmann and Y. Paz, *J. Photochem. Photobiol. A Chem.*, **290**, 11 (2014).
67. G. K. Tripathi and R. Kurchania, *J. Mater. Sci. Mater. Electron.*, **27**, 5079 (2016).
68. E. Sanchez and T. Lopez, *Mater. Lett.*, **25**, 271 (1995).
69. S. Kato, Y. Hirano, M. Iwata, T. Sano, K. Takeuchi and S. Matsuzawa, *Appl. Catal., B: Environ.*, **57**, 109 (2005).
70. R. Asahi, T. Morikawa, T. Ohwaki, K. Aoki and Y. Taga, *Science*, **293**, 269 (2001).
71. C. Di Valentin and G. Pacchioni, *Catal. Today*, **206**, 12 (2013).
72. G. Jiang, X. Li, Z. Wei, T. Jiang, X. Du and W. Chen, *Powder Technol.*, **260**, 84 (2014).
73. G. Jiang, X. Li, Z. Wei, X. Wang, T. Jiang, X. Du and W. Chen, *Powder Technol.*, **261**, 170 (2014).
74. G. H. Jiang, X. Li, Z. Wei, T. T. Jiang, X. X. Du and W. X. Chen, *Acta Metall. Sin.* (English Lett.), **28**, 460 (2015).
75. M. Khan, W. Cao, J. Li, M. I. Zaman and A. Manan, *Int. J. Mod. Phys. B*, **28**, 1450112 (2014).
76. B. Modak, K. Srinivasu and S. K. Ghosh, *J. Phys. Chem. C*, **118**, 10711 (2014).
77. R. Radha, U. N. Gupta, V. Samuel, H. Muthurajan, H. H. Kumar and V. Ravi, *Ceram. Int.*, **34**, 1565 (2008).
78. M. Gao, D. Zhang, X. Pu, X. Shao, H. Li and D. Lv, *J. Am. Ceram. Soc.*, **99**, 881 (2015), DOI:10.1111/jace.14012.
79. Y. Zong, Z. Li, X. Wang, J. Ma and Y. Men, *Ceram. Int.*, **40**, 10375 (2014).
80. M. Haase and H. Schäfer, *Angew. Chem. Int. Ed. Engl.*, **50**, 5808 (2011).
81. J. Xu, Y. Ao, D. Fu and C. Yuan, *J. Colloid Interface Sci.*, **328**, 447 (2008).
82. A. Dash, S. Sarkar, V. N. K. B. Adusumalli and V. Mahalingam, *Langmuir*, **30**, 1401 (2014).
83. X. Jin, L. Ye, H. Wang, Y. Su, H. Xie, Z. Zhong and H. Zhang, *Appl. Catal., B: Environ.*, **165**, 668 (2015).

84. L. Ye, X. Jin, C. Liu, C. Ding, H. Xie, K. H. Chu and P. K. Wong, *Appl. Catal., B: Environ.*, **187**, 281 (2016).
85. Y. Bai, T. Chen, P. Wang, L. Wang and L. Ye, *Chem. Eng. J.*, **304**, 454 (2016).
86. J. Wang, Y. Yu and L. Zhang, *Appl. Catal., B: Environ.*, **136**, 112 (2013).
87. X. Lin, T. Huang, F. Huang, W. Wang and J. Shi, *J. Phys. Chem. B*, **110**, 24629 (2006).
88. S. Sun, W. Wang, L. Zhang, L. Zhou, W. Yin and M. Shang, *Environ. Sci. Technol.*, **43**, 2005 (2009).
89. Y. Su, C. Ding, Y. Dang, H. Wang, L. Ye, X. Jin, H. Xie and C. Liu, *Appl. Surf. Sci.*, **346**, 311 (2015).
90. X. Jin, L. Ye, H. Wang, Y. Su, H. Xie, Z. Zhong and H. Zhang, *Appl. Catal., B: Environ.*, **165**, 668 (2015).
91. L. Xu, Y.-L. Hu, C. Pelligra, C.-H. Chen, L. Jin, H. Huang, S. Sithambaram, M. Aindow, R. Joesten and S. L. Suib, *Chem. Mater.*, **21**, 2875 (2009).
92. J. Xu, L. Li, C. Guo and Y. Zhang, 5th Int. Conf. Bioinforma. Biomed. Eng. iCBBE 2011, 3 (2011).
93. R. Narayanan and M. A. El-Sayed, *Nano Lett.*, **4**, 1343 (2004).
94. D. Zhang, L. Chen, C. Xiao, J. Feng, L. Liao, Z. Wang and T. Wei, *J. Nanomater.*, **33**, 2016 (2016).
95. H. Zhang, Y. Yang, Z. Zhou, Y. Zhao and L. Liu, *J. Phys. Chem. C*, **118**, 14662 (2014).
96. H. Zhang, L. Liu and Z. Zhou, *RSC Adv.*, **2**, 9224 (2012).
97. Y. Bi, S. Ouyang, N. Umezawa, J. Cao and J. Ye, *J. Am. Chem. Soc.*, **133**, 6490 (2011).
98. H. G. Yang, C. H. Sun, S. Z. Qiao, J. Zou, G. Liu, S. C. Smith, H. M. Cheng and G. Q. Lu, *Nature*, **453**, 638 (2008).
99. J. Jiang, K. Zhao, X. Xiao and L. Zhang, *J. Am. Chem. Soc.*, **134**, 4473 (2012).
100. L. Ye, L. Tian, T. Peng and L. Zan, *J. Mater. Chem.*, **21**, 12479 (2011).
101. D.-H. Wang, G.-Q. Gao, Y.-W. Zhang, L.-S. Zhou, A.-W. Xu and W. Chen, *Nanoscale*, **4**, 7780 (2012).
102. D. Zhang, J. Li, Q. Wang and Q. Wu, *J. Mater. Chem. A*, **1**, 8622 (2013).
103. S. Xie, K. Ouyang and X. Ma, *Ceram. Int.*, **40**, 12353 (2014).
104. A. Pimentel, J. Rodrigues, P. Duarte, D. Nunes, F. M. Costa, T. Monteiro, R. Martins and E. Fortunato, *J. Mater. Sci.*, **50**, 5777 (2015).
105. S. Zhang and J. Yang, *Ind. Eng. Chem. Res.*, **54**, 9913 (2015).
106. J. Liu, H. Li, N. Du, S. Song and W. Hou, *RSC Adv.*, **4**, 31393 (2015).
107. J. Hu, G. Xu, J. Wang, J. Lv, X. Zhang, T. Xie, Z. Zheng and Y. Wu, *Dalton Trans.*, **44**, 5386 (2015).
108. V. J. Babu, R. S. R. Bhavatharini and S. Ramakrishna, *RSC Adv.*, **4**, 29957 (2014).
109. H. Shu, K. Sun, H. Li, J. Xia, H. Xu, L. Xu, M. He and J. Di, *Micro Nano Lett.*, **8**, 450 (2013).
110. K. Zhang, J. Liang, S. Wang, J. Liu, K. Ren, X. Zheng, H. Luo, Y. Peng, X. Zou, X. Bo, J. Li and X. Yu, *Cryst. Growth Des.*, **12**, 793 (2012).
111. L. Zhang, X. Yuan, H. Wang, X. Chen, Z. Wu, Y. Liu, S. Gu, Q. Jiang and G. Zeng, *RSC Adv.*, **5**, 98184 (2015).
112. X. Shi, X. Chen, X. Chen, S. Zhou, S. Lou, Y. Wang and L. Yuan, *Chem. Eng. J.*, **222**, 120 (2013).
113. H. Tang, Y. Ao, P. Wang and C. Wang, *Mater. Sci. Semicond. Process*, **27**, 909 (2014).
114. W. Wang, M. He, H. Zhang and Y. Dai, *Int. J. Electrochem. Sci.*, **11**, 1831 (2016).
115. S. Kang, R. C. Pawar, Y. Pyo, V. Khare and C. S. Lee, *J. Exp. Nanosci.*, **8080**, 1 (2015).
116. K. Dai, T. Peng, D. Ke and B. Wei, *Nanotechnology*, **20**, 125603 (2009).
117. S. Wang and S. Zhou, *J. Hazard. Mater.*, **185**, 77 (2011).
118. B. Weng, F. Xu and J. Xu, *J. Nanopart. Res.*, **16**, 2766 (2014).
119. F. Deng, X. Lu, F. Zhong, X. Pei, X. Luo, S. Luo, D. D. Dionysiou and C. Au, *Nanotechnology*, **27**, 65701 (2016).
120. J. Di, J. Xia, M. Ji, B. Wang, S. Yin, H. Xu, Z. Chen and H. Li, *Langmuir*, **32**, 2075 (2016).
121. J. Di, J. Xia, M. Ji, L. Xu, S. Yin, Q. Zhang, Z. Chen and H. Li, *Carbon N. Y.*, **98**, 613 (2016).
122. Y. Chen, Q. Lu, X. Yan, Q. Mo, Y. Chen, B. Liu, L. Teng, W. Xiao, L. Ge and Q. Wang, *Nanoscale Res. Lett.*, **11**, 60 (2016).
123. Y. Bai, P.-Q. Wang, J.-Y. Liu and X.-J. Liu, *RSC Adv.*, **4**, 19456 (2014).
124. S. Vadivel, V. P. Kamalakannan, N. P. Kavitha, T. Santhoshini Priya and N. Balasubramanian, *Mater. Sci. Semicond. Process.*, **41**, 59 (2016).
125. O. Mehraj, N. A. Mir, B. M. Pirzada and S. Sabir, *Appl. Surf. Sci.*, **332**, 419 (2015).
126. C. Liao, Z. Ma, G. Dong and J. Qiu, *Appl. Surf. Sci.*, **314**, 481 (2014).
127. Y. Liu, W. Yao, D. Liu, R. Zong, M. Zhang, X. Ma and Y. Zhu, *Appl. Catal., B: Environ.*, **163**, 547 (2015).
128. L. Kong, Z. Jiang, T. Xiao, L. Lu, M. O. Jones and P. P. Edwards, *Chem. Commun. (Camb)*, **47**, 5512 (2011).
129. S. Shamaila, A. K. L. Sajjad, F. Chen and J. Zhang, *J. Colloid Interface Sci.*, **356**, 465 (2011).
130. D. Yue, D. Chen, Z. Wang, H. Ding, R. Zong and Y. Zhu, *Phys. Chem. Chem. Phys.*, **16**, 26314 (2014).
131. J. Cao, B. Xu, B. Luo, H. Lin and S. Chen, *Catal. Commun.*, **13**, 63 (2011).
132. J. Cao, B. Xu, H. Lin, B. Luo and S. Chen, *Chem. Eng. J.*, **185**, 91 (2012).
133. J. Zhang, J. Xia, S. Yin, H. Li, H. Xu, M. He, L. Huang and Q. Zhang, *Colloids Surf. A Physicochem. Eng. Asp.*, **420**, 89 (2013).
134. Z. Liu, H. Ran, B. Wu, P. Feng and Y. Zhu, *Colloids Surf. A Physicochem. Eng. Asp.*, **452**, 109 (2014).
135. Y. R. Jiang, S. Y. Chou, J. L. Chang, S. T. Huang, H. P. Lin and C. C. Chen, *Rsc Adv.*, **5**, 30851 (2015).
136. X. Xiao, R. Hao, M. Liang, X. Zuo, J. Nan, L. Li and W. Zhang, *J. Hazard. Mater.*, **233-234**, 122 (2012).
137. X. jing Wang, Q. Wang, F. tang Li, W. yan Yang, Y. Zhao, Y. juan Hao and S. Jun Liu, *Chem. Eng. J.*, **234**, 361 (2013).
138. H. Liu, W. Cao, Y. Su, Y. Wang and X. Wang, *Appl. Catal., B: Environ.*, **111-112**, 271 (2012).
139. X. Li, X. Mao, X. Zhang, Y. Wang, Y. Wang, H. Zhang, X. Hao and C. Fan, *Sci. China Chem.*, **58**, 457 (2015).
140. L. Ye, J. Liu, C. Gong, L. Tian, T. Peng and L. Zan, *ACS Catal.*, **2**, 1677 (2012).

141. C. Yu, F. Cao, G. Li, R. Wei, J. C. Yu, R. Jin, Q. Fan and C. Wang, *Sep. Purif. Technol.*, **120**, 110 (2013).
142. M. Zhu, P. Chen and M. Liu, *ACS Nano*, **5**, 4529 (2011).
143. Y. Zhang, Z.-R. Tang, X. Fu and Y.-J. Xu, *Appl. Catal., B: Environ.*, **106**, 445 (2011).
144. L. Zhang, K.-H. Wong, Z. Chen, C. Y. Jimmy, J. Zhao, C. Hu, C.-Y. Chan and P.-K. Wong, *Appl. Catal., A: Gen.*, **363**, 221 (2009).
145. L.-S. Zhang, K.-H. Wong, H.-Y. Yip, C. Hu, J. C. Yu, C.-Y. Chan and P.-K. Wong, *Environ. Sci. Technol.*, **44**, 1392 (2010).
146. P. Wang, B. Huang, Q. Zhang, X. Zhang, X. Qin, Y. Dai, J. Zhan, J. Yu, H. Liu and Z. Lou, *Chem. Eur. J.*, **16**, 10042 (2010).
147. P. Wang, B. Huang, X. Qin, X. Zhang, Y. Dai, J. Wei and M. Whangbo, *Angew. Chem. Int. Ed.*, **47**, 7931 (2008).
148. P. Wang, B. Huang, Z. Lou, X. Zhang, X. Qin, Y. Dai, Z. Zheng and X. Wang, *Chem. Eur. J.*, **16**, 538 (2010).
149. G. Tian, Y. Chen, H.-L. Bao, X. Meng, K. Pan, W. Zhou, C. Tian, J.-Q. Wang and H. Fu, *J. Mater. Chem.*, **22**, 2081 (2012).
150. Y. Li and Y. Ding, *J. Phys. Chem. C*, **114**, 3175 (2010).
151. M. R. Elahifard, S. Rahimnejad, S. Haghighi and M. R. Gholami, *J. Am. Chem. Soc.*, **129**, 9552 (2007).
152. C. An, S. Peng and Y. Sun, *Adv. Mater.*, **22**, 2570 (2010).
153. T. Yan, X. Yan, R. Guo, W. Zhang, W. Li and J. You, *Catal. Commun.*, **42**, 30 (2013).
154. W. Xiong, Q. Zhao, X. Li and D. Zhang, *Catal. Commun.*, **16**, 229 (2011).
155. T. Li, S. Luo and L. Yang, *J. Solid State Chem.*, **206**, 308 (2013).
156. T. Li, S. Luo and L. Yang, *Mater. Lett.*, **109**, 247 (2013).
157. Y. Lei, G. Wang, P. Guo and H. Song, *Appl. Surf. Sci.*, **279**, 374 (2013).
158. H. Cheng, B. Huang, P. Wang, Z. Wang, Z. Lou, J. Wang, X. Qin, X. Zhang and Y. Dai, *Chem. Commun.*, **47**, 7054 (2011).
159. J. Cao, Y. Zhao, H. Lin, B. Xu and S. Chen, *J. Solid State Chem.*, **206**, 38 (2013).
160. K. Kolwas, A. Derkachova and M. Shopa, *J. Quant. Spectrosc. Radiat. Transf.*, **110**, 1490 (2009).
161. K.-H. Kim, A. Husakou and J. Herrmann, *Opt. Express*, **18**, 7488 (2010).
162. T. Atay, J.-H. Song and A. V. Nurmikko, *Nano Lett.*, **4**, 1627 (2004).
163. J. J. Mock, M. Barbic, D. R. Smith, D. A. Schultz and S. Schultz, *J. Chem. Phys.*, **116**, 6755 (2002).
164. W. Hou and S. B. Cronin, *Adv. Funct. Mater.*, **23**, 1612 (2013).
165. H. Choi, W. T. Chen and P. V. Kamat, *ACS Nano*, **6**, 4418 (2012).
166. A. Pron and P. Rannou, *Prog. Polym. Sci.*, **27**, 135 (2002).
167. Q. Wang, J. Hui, J. Li, Y. Cai, S. Yin, F. Wang and B. Su, *Appl. Surf. Sci.*, **283**, 577 (2013).
168. J. Xiao, W. Chen, F. Wang and J. Du, *Macromolecules*, **46**, 375 (2013).
169. G. Liao, S. Chen, X. Quan, H. Chen and Y. Zhang, *Environ. Sci. Technol.*, **44**, 3481 (2010).
170. S. Horikoshi, N. Serpone, Y. Hisamatsu and H. Hidaka, *Environ. Sci. Technol.*, **32**, 4010 (1998).
171. F. Chang, J. Luo, X. Wang, Y. Xie, B. Deng and X. Hu, *J. Colloid Interface Sci.*, **459**, 136 (2015).
172. C. Chen, X. Li, W. Ma, J. Zhao, H. Hidaka and N. Serpone, *J. Phys. Chem. B*, **106**, 318 (2002).
173. L. Yu, X. Zhang, G. Li, Y. Cao, Y. Shao and D. Li, *Appl. Catal., B: Environ.*, **187**, 301 (2016).
174. X. Mao, C. Fan, Y. Wang, Y. Wang and X. Zhang, *Appl. Surf. Sci.*, **317**, 517 (2014).
175. G. Li, B. Jiang, S. Xiao, Z. Lian, D. Zhang, J. C. Yu and H. Li, *Environ. Sci. Process. Impacts*, **16**, 1975 (2014).

Supporting Information

A review and recent developments on strategies to improve the photocatalytic elimination of organic dye pollutants by BiOX (X=Cl, Br, I, F) nanostructures

Sonal Singh[*,‡], **Rishabh Sharma**[**,‡], **and Manika Khanuja**[***,†]

*Shaheed Rajguru College of Applied Sciences for Women, University of Delhi, New Delhi 110096, India
**Thin Film Laboratory, Department of Physics, Indian Institute of Technology, New Delhi-110016, India
***Centre for Nanoscience and Nanotechnology, Jamia Millia Islamia, New Delhi-110025, India
(*Received 3 May 2018 • accepted 24 June 2018*)

Table S1. Summary of literature on photocatalytic BiOCl over various types of organic pollutants

Material	Morphology/ Band gap (eV)	Light source	Pollutant	Experimental conditions			Photo degradation efficiency (%)	Synthesis method	Ref.
Pure				PC (g/L)	Pollutant (mg/L)*	Irradiation time			
BiOCl	Plates 3.46	300 W UV mercury lamp	Methyl orange (MO)	2	10	10 min	Complete degradation	Hydrolysis	[1]
BiOCl	Plates 3.43	500 W mercury lamp (UV)/500 W xenon lamp (Vis)	Methyl orange (MO)	1	10	60 min	98.97 (UV)	Hydrolysis	[2]
			Rhodamine B (RhB)	1	10	60 min	100 (UV, Vis)		
			Methylene blue (MB)	1	10	60 min	96.36 (UV)		
			Alizarin green (AR)	1	10	60 min	95.91 (UV)		
BiOCl	Fine ferrite plates -	500 W xenon lamp	Methyl orange (MO)	1	10	150 min	98.50	Hydrolysis	[3]
BiOCl	Nanodisk 3.11	350 W xenon arc lamp	Rhodamine B (RhB)	0.6	20	120 min	Complete degradation	Facile approach with a mixture of solvent EG and water	[4]
BiOCl	Ferrite plate 3.3	500 W xenon lamp	Methyl orange (MO)	1	10	160 min	—	Hydrolysis	[5]
BiOCl	Nanosheets 3.05-3.27	100 W mercury lamp	Rhodamine B (RhB)	0.1	10	60 min	Complete degradation	Solvothermal	[6]
BiOCl	Nanoflakes 3.11-3.27	100 W mercury lamp	Rhodamine B (RhB)	1	20	75 min	99.50	Hydrolysis	[7]

Table S1. Continued

Material	Morphology/ Band gap (eV)	Light source	Pollutant	Experimental conditions			Photo degradation efficiency (%)	Synthesis method	Ref.
Pure				PC (g/L)	Pollutant (mg/L)*	Irradiation time			
BiOCl	Nanosheets ~3 ev	150 W Xe	Rhodamine B (RhB)	0.05	10^{-5} M	20 min	98	Chemical route	[8]
BiOCl	Microflowers 3.33	500 W mercury vapor lamp	Rhodamine B (RhB) Natural red 4 (N-Red)	0.5 0.5	10 10	5 h 5 h	78.12 55.54	Microwave assisted	[9]
BiOCl {001 facet}	Nanosheets 3.22	500 W xenon lamp	Rhodamine B (RhB) Methylene blue (MB) Methyl orange (MO)	1 1 1	20 10 10	30 min 2 hrs 2 hrs	94 27 79	Hydrolysis	[10]
BiOCl {001 facet}	Nanoplates 3.15	500 W xenon lamp	Rhodamine B (RhB)	0.2	10	30 min	80	Electrochemical (anodic oxidation)	[10]
BiOCl (with 'x' min milling)	Nanoplates 2.77-3.27	500 W mercury vapor lamp	Rhodamine B (RhB)	0.5	10 mg dm^{-3}	4 hrs	15 min=97 30 min=60 60 min=78	Mechanochemical synthesis	[11]
Composite/heterostructure									
BiOCl/Bi2MoO6	Nanoplates/nanosheets —	Visible light irradiation	Methyl orange (MO) Phenol	1	10	80 min 4 hrs	82.1 40.2	Hydrothermal	[12]
x % $BiPO_4$/ BiOCl	Cuboids and bulk plates 3.16-3.23	500 W Axe lamp	Methyl orange (MO)	1	10	14 min	30%=87 40%=98 50%=82	Hydrothermal	[13]
BiOCl/ZnO	Nanoflowers 3.18-3.24	300 W Hg lamp	Rhodamine B (RhB)	1	40	140 min	Complete degradation	Solvothermal	[14]
Cu_2O/BiOCl	Plates and particles —	300 W Hg lamp (UV) light/300 W xenon lamp (Vis)	Rhodamine B (RhB)	Thin film	—	120 min	—	Sol-gel dip-coating technique and magnetron sputtering	[15]
BiOCl/Bi_3O_4Cl	Sheets and nano-grains —	300 W xenon lamp	2-Propanol (IP) Salicylic acid (SA)	Thin film	0.08 mL	120 min 120 min	—	Wet-chemical process	[16]
Ag/$AgVO_3$/BiOCl	Flower-like structure BiOCl=3.12, Ag/$AgVO_3$=2.10	300 W xenon lamp	Methylene blue (MB)	0.5	7	60 min	93.16	Hydrothermal	[17]
BiOCl/Ag_3PO_4 (1 : 0.1)	Plates and particles —	500 W Hg lamp	Methylene blue (MB)	0.06	10	260 min	92	Hydrothermal	[18]

Table S1. Continued

Material	Morphology/ Band gap (eV)	Light source	Pollutant	Experimental conditions			Photo degradation efficiency (%)	Synthesis method	Ref.
Pure				PC (g/L)	Pollutant (mg/L)*	Irradiation time			
BiOCl/BHO	Flake-type 2.81-3.31	300 W xenon arc lamp	Rhodamine B (RhB) Acetophenone (AP)	0.5 0.5	15 ppm 120 ppm	<1 hr 4 hrs	Complete degradation 30	Hydrothermal	[19]
x% WO_3/BiOCl	Nanoflakes —	1000 W halogen lamp	Rhodamine B (RhB)	1	30	180 min	10%=100	Hydrolysis	[20]
BiOCl/CuPc	Plate like —	500 W xenon lamp	Rhodamine B (RhB)	1	10^{-5} mol/L	2 h	Complete degradation	Chemical route	[21]
α-Bi_2O_3/BiOCl	Nanosheets Bi_2O_3=2.98, BiOCl=3.27	500 W xenon lamp	Methylene blue (MB)	—	0.03125 mM	270 min	—	Chemical transformation method	[22]
x% Bi_2MoO_6/BiOCl	Irregular multi-plates Bi_2MoO_6=2.6	500 W xenon lamp	Rhodamine B (RhB)	1	10	300 min	30%=highest	Hydrothermal	[23]
x wt% Bi_2O_3-BiOCl	Nanofibers 3.3	UV (<390 nm)	Alizarin red S (ARS)	0.1	10	80 min	1 wt%=88.54 2 wt%=96.94 3 wt%=99.34 4 wt%=92.34	Electro spining	[24]
x M KBH_4- Bi_2O_3/BiOCl	Nanoparticles/sheets 3.44	300 Mercury Lamp	Methyl orange (MO)	1	40	8 min	0.01 M=76.2 0.02 M=95.7 0.03 M=88.6 0.04 M=79.7 0.05 M=66.1	Solvothermal	[25]
x M BiOCl/$BiVO_4$	Microsheets BiOCl=3.44, $BiVO_4$=2.38	500 W xenon lamp	Methyl orange (MO)	1	8	11 hrs	0.75 M=85	Hydrothermal	[26]
Carbon based									
rGO(5 wt%)-(U)BiOCl	Nanosheets 3.22	Xenon arc lamp	Rhodamine B (RhB)	0.1	10	3.5 min	96	Hydrothermal	[27]
BiOCl-g-C_3N_4	Nanoparticles 2.77	300 W xenon lamp	Rhodamine B (RhB)	0.04	10	60 min	99	Chemical bath method	[28]
BiOCl-GR (x%)	Nanoplates —	300 W xenon lamp	Methylene blue (MB)	0.8	35 ppm	75 min	30%=97	Solvothermal	[29]
BiOCl-carbon nanofiber	Nano fiber —	50 W mercury lamp	4-Nitrophenol (4-NP)	0.5	20	30 min	100	Solvothermal/ electrospining	[30]

Table S1. Continued

Material	Morphology/ Band gap (eV)	Light source	Pollutant	Experimental conditions			Photo degradation efficiency (%)	Synthesis method	Ref.
Pure				PC (g/L)	Pollutant (mg/L)*	Irradiation time			
BiOCl/carbon quantum dot (50-150 nm)	Flower like 3.32-3.48	300 W xenon lamp	2-Nitrophenol (2-NP)	1	10	120 min	100	Co-precipitation	[31]
BiOCl-RGO	Sheet like —	100 W halogen lamp	Rhodamine B (RhB)	0.4	4	130 min	Complete degradation	Hydrothermal	[32]
Doped material									
Flourine (x mmol NaF)	Nanosheets 3.44-3.52	300 W xenon lamp	Rhodamine B (RhB)	1	10	35 min	0 mmol=78.9 1 mmol=78.4 2 mmol=98.3 3 mmol=99.7 4 mmol=95.1 5 mmol=81.7	Hydrothermal	[33]
Nb	Needle 2.85-3.4	40 W tungsten lamp	Rhodamine B (RhB)	0.6	15	—	—	Co-precipitation	[34]
Fe	Platelets, needle like, particles —	40 W tungsten lamp	Rhodamine B (RhB)	0.6	15	—	—	Co-precipitation	
Fe,Nb	Platelets, nanoparticles 2.85 to 3.4	40 W tungsten lamp	Rhodamine B (RhB)	0.6	15	—	—	Co-precipitation	
La,Nb	Non-regular 2.85 to 3.4	40 W tungsten lamp	Rhodamine B (RhB)	0.6	15	—	—	Co-precipitation	
In,Nb	Non-regular 2.85 to 3.4	40 W tungsten lamp	Rhodamine B (RhB)	0.6	15	—	—	Co-precipitation	
Sn (x%)	Lamellar 2.91	350 W xenon lamp	Benzoic acid (BA)	1	10	180 min	10%=75	Oxidation-reduction	[35]
Nitrogen	Flower-like —	500 W xenon lamp	Rhodamine B (RhB)	0.001	10	7 hrs	—	Hydrothermal	[36]
Iodine	Core-shell micro-sphere 2.31	Visible light irradiation	Rhodamine B (RhB)	—	20	90 min	99.00	Co-precipitation	[37]
Eu^{3+}	Nanoflakes 2.4-2.6	300 W mercury lamp	Rhodamine B (RhB)	0.1	20	120 min	Complete degradation	Combustion method	[38]

Table S1. Continued

Material	Morphology/ Band gap (eV)	Light source	Pollutant	Experimental conditions			Photo degradation efficiency (%)	Synthesis method	Ref.
Pure				PC (g/L)	Pollutant (mg/L)*	Irradiation time			
Carbon	Flowerlike 3.12	300 W xenon lamp	Phenol	0.2	10^{-5} mol/L	40 min	~70	Wet-chemical method	[39]
Silver (Ag) Nickel (Ni) Vanadium (V)	Flower like —	UV-vis light source	Methylene blue (MB)	0.5	10	5 h 5 h 5 h	Ag=85 Ni=80 V=80	Wet-chemical method	[40]
Iodine (I)	Hollow core shell, solid μspheres 2.04-2.43	75 W halogen tungsten lamp	Rhodamine B (RhB)	1	20	90 min	99	Co-precipitation	[41]
Polymer Assisted									
x wt% PANI/BiOCl	Plates/particles 3.21 eV	500 W xenon arc lamp	Methyl orange (MO)	1	10	210 min	7 wt%=67 9 wt%=59.31	Chemisorption	[42]
PVP assisted BiOCl	Flower-like 2.53-2.57	400 W halogen lamp	Rhodamine B (RhB)	1	10	150 min	Complete degradation	Hydrothermal	[43]

Table S2. Summary of literature on photocatalytic BiOBr over various types of organic pollutants

Material	Morphology/ band gap (eV)	Light source	Pollutant	Experimental conditions			Photo degradation efficiency (%)	Method	Ref.
Pure				PC (g/L)	P (mg/L)*	Irradiation time			
BiOBr (Br : Bi)	Nanosheets —	300 W xenon lamp	Rhodamine B (RhB)	1	15	35 min	2 : 1=91.1 1 : 1=95.9 1 : 2=88.6	Solvothermal	[44]
BiOBr (x-% BiBr3)	Lamellar 2.78-2.81	150 W xenon lamp	Alizarin red S (ARS)	—	—	100 min	1%=80.35 2%=83.89 3%=82.27 4%=67.94	Electrospining	[45]
BiOBr	Flower like 2.64	300 W UV Hg lamp 350 xenon lamp	Toulene	Coating	Vapours	5 hrs	90	Solvothermal	[46]
BiOBr	Micro-nanosheets —	250 W UV lamp	Methyl orange (MO)	10	10	2.5 hrs	98.50	Alcoholysis coating method	[47]

Table 2. Continued

Material	Morphology/ band gap (eV)	Light source	Pollutant	Experimental conditions			Photo degradation efficiency (%)	Method	Ref.
Pure				PC (g/L)	P (mg/L)*	Irradiation time			
BiOBr	Irregular plates/rods 2.22-2.76	20 W vis lamp	Crystal violet (CV)	0.5	100 ppm	48 hrs	99.90	Hydrothermal	[48]
BiOBR ($CTAB : Bi(NO_3)_3$)	Lamellar 2.78-2.81	500 W xenon lamp	Methyl orange (MO)	1	10	120 min	2 : 1=96 3 : 1=80 4 : 1=72 5 : 1=83	Hydrothermal	[49]
BiOBr	Microspheres	Visible light (λ>420 nm)	Methylene blue (MB) Cr(VI)	2.5 1.4	320 37	6 hrs 6 hrs	55 90	Ionothermal	[50]
BiOBr	Nanosheets 2.24-2.61	800 W xenon lamp	Rhodamine B (RhB)	0.5	1	60 min	100	Solvothermal	[51]
BiOBr	Flake like 2.92	300 W xenon lamp	Methyl orange (MO)	2	10	6 hrs	—	Hydrothermal	[52]
BiOBr	Microspheres 2.75-2.96	500 W tungsten halogen lamp	Rhodamine B (RhB) Methyl orange (MO) 4-Chlorophenol (4-CP)	0.5 0.5 0.5	2.5×10^{-5} mol/L 10 10	60 min 60 min 60 min	—	Solvothermal	[53]
BiOBr	Nanoplates 2.76	Visible light (λ>420 nm)	Sulforhodamine (SRB) Salicylic acid (SA)	0.8 0.8	1.5×10^{-5} mol/L 25 ml	150 min 8 hrs	100 97	Hydrothermal	[54]
BiOBr	Flower like 2.72-2.77	300 W xenon lamp	Rhodamine B (RhB)	0.2	10	60 min	99%	Solvothermal	[55]
BiOBR (x grinding min)	Nanoplates 2.74/3.25	500 W mercury-vapor lamp	Rhodamine B (RhB) Pentachlorophenol (PCB)	0.5 0.5	10 10	4 hrs 60 min	15 min=66.49 (RhB) 30 min=91.43 (RhB) 60 min=86.27 (RhB) 30 min=99 (PCB)	Mechanochemical	[56]
BiOBr	Sphere like 2.26/2.29	150 W tungsten halogen lamp	Rhodamine B (RhB)	0.2	10	105 min	Microsphere=79 Flower=97	Solvothermal	[57]
BiOBr	Nanosheets 2.54	300 W xenon arc lamp	Methyl orange (MO)	1	10	5 hrs	Complete degradation	Solvothermal	[58]
BiOBr	Nanosheets 2.66-2.77	500 W xenon arc lamp	Methyl orange (MO) Rhodamine B (RhB)	1 5	10 10	50 min 30 min	98.10 98.64	Solvothermal	[59]

Table 2. Continued

Material	Morphology/ band gap (eV)	Light source	Pollutant	Experimental conditions			Photo degradation efficiency (%)	Method	Ref.
Pure				PC (g/L)	P (mg/L)*	Irradiation time			
BiOBr {102}	Nanosheets {001}-1.44, {102}-2.22	350 W xenon lamp	Rhodamine B (RhB)	0.1	2×10^{-5} mol/L	16 min	Complete degradation	Hydrothermal	[60]
BiOBr	Flower like 2.9	500 W xenon lamp	Rhodamine B (RhB)	0.5	20	50 min	Complete degradation	Solvothermal	[61]
Composite/heterostructure									
x ml NaOH-BiOBr/$Bi_{24}O_{31}Br_{10}$	Nanosheets 2.23-2.64	150 W tungsten halogen lamp	Rhodamine B (RhB)	1	15	2 hrs	0 ml=89.6 1 ml=98.1 1.5 ml=99.7 2 ml=95.8 3 ml=76.6	Solvothermal	[62]
BiOBr/TiO_2-X (Ti/Bi molar ratio)	Flakes 2.66-2.99	300 W xenon lamp	Rhodamine B (RhB)	2.5	10	20 min	10 molar ratio=100 5 molar ratio=92	Solvothermal	[63]
Pt-BiOBr	Micropheres/sphere-like micro flowers 2.9	Visible light (λ>400 nm)	p-Nitrophenol (PNP) Tetrabromobisphenol-A (TBBPA)	1 1	10 10	90 min 15 min	Micro sphere=99.1 micro flowers=93.5 Nanosheets=90.4 Micro spheres=98.4 (TBBPA)	Hydro(solvo) thermal	[64]
x : y BiOBr-CdS	Core-satellite structure BiOBr=2.55, CdS=2.34	500 W xenon lamp	Bisphenol A (BPA)	1	20	5 hrs	1 : 5=78	Crystallization approach	[65]
x wt% BiOBr/ZnO	Hour glass like structure 3	300 W halogen tungsten lamp	Rhodamine B (RhB)	0.5	0.001	90 min	50 wt%=97	Hydrothermal	[66]
Fe_3O_4/BiOBr	Microspheres —	300 W xenon lamp	Rhodamine B (RhB)	0.5	1×10^{-5} M	100 min	Complete degradation	Solvothermal	[67]
x % AgBr/BiOBr	Flower like BioBr=2.60, AgBr=2.39	500 W xenon lamp	Methyl orange (MO)	2	10	180 min	50%=highest	Deposition-precipitation	[68]
x-BiOBr/y-$ZnFe_2O_4$	Micro spherical 1.71-2.25	Visible-light irradiation	Rhodamine B (RhB)	1	20	10 min	0.1-0.9=73	Deposition-precipitation	[69]

Table 2. Continued

Material	Morphology/ band gap (eV)	Light source	Pollutant	Experimental conditions			Photo degradation efficiency (%)	Method	Ref.
Pure				PC (g/L)	P (mg/L)*	Irradiation time			
$Fe_3O_4/mSiO_2/BiOBr$	Microspheres —	500 W xenon lamp	Methylene blue (MB)	1	20	120 min	96	Solvothermal	[70]
Ag/BiOBr	Nanosheets 2.40-2.92	500 W xenon lamp	Methyl orange (MO) Phenol	0.2 0.5	10 10	120 min 150 min	98.6 86	Photo reduction method	[71]
x-BiOBr/y-BHO	Platelets 2.63-2.69	300 W xenon arc lamp	Rhodamine B (RhB) Acetophenone (AP)	0.5 0.5	15 ppm 120 ppm	50 min 4 h	0.9-0.1= Complete degradation 0.9-0.1=70	Hydrothermal/ hydrolysis	[72]
$BiOBr-Bi_2WO_6$	Nanosheets —	3 W LED lamp (400-405 nm)	Rhodamine B (RhB) Methyl orange (MO)	1 1	2×10^{-5} M 2×10^{-5} M	40 min —	81.4 —	Hydrothermal	[73]
Carbon based									
N-doped BiOBr/CFs	Nanosheets —	500 W xenon lamp	Rhodamine B (RhB) Methanol	0.6 0.6	10 50 ml	60 min 2.5 hrs	— 90	Solvothermal	[74]
GO-BiOBr	Flake like 1.91	150 W tungsten lamp	Methylene blue (MB)	0.6	25-150	2 hrs	96.84	Chemical route	[75]
CNTs/BiOBr	Flowers like —	White LED (100 W)	Rhodamine B (RhB)	0.3	20	4 hrs	>95	Hydrothermal	[76]
$x-BiOBr/y-C_3N_4$	Nanoflakes —	300 W xenon lamp	Rhodamine B (RhB)	0.5	20	10 min	0.5-0.5>60	Chemical & physical route	[77]
$BiOBr/TiO_2$/graphene	Nanoparticles —	300 W xenon lamp	Rhodamine B (RhB)	0.25	10	50 min	—	One-pot approach	[78]
Doped									
Ti	Microspheres 2.54	11 W daylight lamp (25 Hz)	Rhodamine B (RhB)	1	10	3 hrs	Complete degradation	Double self-assemble method	[79]
x %Fe–BiOBr	Micro-flower —	150 W tungsten halogen lamp	Methyl orange (MO)	1	10	200 min	15%=highest	Solvothermal	[80]
Fe	Hollow microspheres 1.67	11 W daylight lamp (25 Hz)	Rhodamine B (RhB)	1	10	30 min	75	Solvothermal	[81]
Iodine (x pH)	Fower-like microspheres 2	500 W xenon lamp	Methyl orange (MO) Phenol	2 2	10 10	3 hrs 8 hrs	0.5=96 0.5=51	Chemical precipitation	[82]

Table 2. Continued

Material	Morphology/ band gap (eV)	Light source	Pollutant	Experimental conditions			Photo degradation efficiency (%)	Method	Ref.
Pure				PC (g/L)	P (mg/L)*	Irradiation time			
N and/or S	Flower-like 1.61-1.91	11 W daylight lamp (25 Hz)	Rhodamine B (RhB)	0.4	—	1 hr	Complete degradation	Solvothermal	[83]
Polymer assisted									
x gm PVP-BiOBr	Flower-like 1.75-2.5	300 W tungsten lamp	Methyl orange (MO)	1	10	100 min	0 gm=60 0.05 gm=80 0.1 gm=96 0.2 gm=98	Hydrothermal	[84]

*Certain values mentioned in mol, M or ppm

Table S3. Summary of literature on photocatalytic BiOI over various types of organic pollutants

Material	Morphology/ Band gap (eV)	Light source	Pollutant	Experimental conditions			Photo degradation efficiency (%)	Synthesis method	Ref.
Pure				PC (g/L)	Pollutant (mg/L)*	Irradiation time			
BiOI	Plate like 1.71-1.88	Visible light (λ>420 nm)	Methyl orange (MO)	0.8	50	180 min	90	Hydrolysis	[85]
BiOI	Nano plates 2.12	300 W tungsten halogen lamp	Acid orange II (AO)	0.625	20	120 min	—	Solution combination with thermal treatment	[86]
BiOI	Nano plates 1.85	500 W xenon lamp	Methyl orange (MO) Phenol	1 1	10 20	60 min 4 hrs	97 55	Precipitation filteration	[87]
BiOI	Nano sheets No data	Simulated solar irradiation	Sodium pentachlorophenate (PCP- Na)	1.5	50 ppm	1 hr	90.3	Chemical route	[88]
BiOI	Nano sheets 1.82	500 W xenon lamp	Rhodamine B (RhB) Phenol	1 1	5×10^{-5} mol/L 1×10^{-4} mol/L	15 240	—	Chemical route	[89]
BiOI	Flower like 1.83	500 W xenon lamp	Methylene blue (MB) Methyl orange (MO) Rhodamine B (RhB)	0.5 0.5 0.5	0.01 mM 0.01 mM 0.01 mM	3 hrs 3 hrs 3 hrs	30 60 Complete degradation	Solution route	[90]

Table 3. Continued

Material	Morphology/ Band gap (eV)	Light source	Pollutant	Experimental conditions			Photo degradation efficiency (%)	Synthesis method	Ref.
Pure				PC (g/L)	Pollutant (mg/L)*	Irradiation time			
BiOI(@160 C, 30 hrs)	Flower like 1.81	400 W metal halide lamp	Rhodamine B (RhB)	0.2	10	50 min	88	Hydrothermal	[91]
BiOI	Nanoplatelets 1.85-1.87	Visible light	Phenol	1	25	4 hrs	Spheres=97 Platelets=62	Facile method	[92]
BiOI	Micro plates 1.7	300 W xenon lamp	Rhodamine B (RhB) Methyl orange (MO) Phenol	0.2 0.2 0.2	2.0×10^{-5} M 2.0×10^{-5} M 2.0×10^{-4} M	15 min 15 min 60 min	40 94 70	Hydrothermal	[93]
BiOI	Thin sheets/ plates/rods 1.86-3.31	150 W xenon arc lamp	Crystal violet (CV)	0.5	10 ppm	24 hrs	99.9	Hydrothermal	[94]
BiOI P-BiOI (without ionic liquid) M-BiOI (Hierarchical BiOI) IL-BiOI (Ionic Liquid)	Nanoplates 1.72-1.77	500 W tungsten halogen lamp	Methyl orange (MO)	1	10	3 hrs	P-BiOI=27 M-BiOI=78 IL-BiOI=87	Chemical precipitation and sol gel	[95]
Composite/heterostructure									
x% $BiOI/TiO_2$	Slice-like 1.74-1.83	250 W halogen lamp	Methyl orange (MO)	0.5	10	3 hrs	25%=64 50%=85 75%=92 100%=54	Two microemulsion approach	[96]
$BiOI/TiO_2$	Fibers 1.86	500 W xenon lamp	Rhodamine B (RhB)	1	20	135 min	92	Hydrothermal	[97]
x% Ag/BiOI	Lamellar 1.66-1.72	500 W xenon arc lamp	Acid orange II (AO) Methyl orange (MO) Rhodamine B (RhB)	1 1 1	10 10 10	4 hrs 4 hrs 4 hrs	0.6%=92.1 0.6%=80.0 0.6%=49.6	Hydrothermal & photo deposition	[98]
x% $BiPO_4$/BiOI	Nano sheets/rods No data	500 W xenon lamp	Phenol total organic compound (TOC)	0.5 -	25 ppm -	5 hrs 5 hrs	7%=45.8 7%=27.9	Hydrothermal	[99]
x% $BiOI\text{-}TiO_2$	Sheet structure 1.9-3.2	250 W halogen lamp	Bisphenol A (BPA)	0.5	20	90 min	25%=47.1 50%=62.5 75%=82.5 100%=24.9	Microemulsion	[100]

Table 3. Continued

Material	Morphology/ Band gap (eV)	Light source	Pollutant	Experimental conditions			Photo degradation efficiency (%)	Synthesis method	Ref.
Pure				PC (g/L)	Pollutant (mg/L)*	Irradiation time			
BiOI/montmorillonite	Nanoplates 1.71-1.76	300 W xenon arc lamp	Methylene blue (MB)	1	10	45 min	95	Facile room temperature method	[101]
x% AgI/BiOI	Flower, microspheres AgI=2.77 BiOI=1.78	500 W tungsten lamp	Phenol Rhodamine B (RhB)	1 1	10 10	100 min 120 min	0.4%=95.4 0.4%=100	Ion exchange reaction	[102]
Carbon based									
x wt% CQDs/BiOI	Sphere like BiOI=1.81	300 W xenon lamp	Rhodamine B (RhB)	0.3	10	120 min	6 wt%=94.9	Solvothermal	[103]
x wt% GR/BiOI	Nanosheets/plates 1.50-1.54	500 W xenon lamp	Methyl orange (MO)	1	10	4 hrs	1 wt%=75.7 2 wt%=88.0 3 wt%=67.8	Hydrothermal	[104]
BiOI-GO	Nanoflowers BiOI=1.97	350 W xenon lamp	Phenol	Thin film	100	150 min	-	Self assembly approach	[105]
x wt% CQDs/BiOI	Nanosheets 1.45	300 W xenon lamp	Tetracycline (TC) Rhodamine B (RhB) Bisphenol A (BPA)	0.5 0.3 1	20 10 10	30 min 120 min 120 min	3 wt%=59 (TC) 0.5 wt%=37.8 (TC) 3 wt%=43.1 (TC) 5 wt%=47.5 (RhB) 3 wt%=99 (BPA)	Room temperature chemical method	[106]
x wt% CQDs/BiOI	Nanoplates BiOI-1.8	150 W xenon lamp	Methyl orange (MO)	1	50	50 min	1.5 wt%=98	Hydrothermal	[107]
Doped									
x mol% Ag	Microflowers 2.08	450 W xenon lamp	Methyl orange (MO)	1	10^{-5} M	180 min	0.5 mol%=58.06 3 mol%=70.87 1 mol%=91.26	Hydrothermal	[108]

*Certain values mentioned in mol, M or ppm

Table S4. Summary of literature on photocatalytic BiOF over various types of organic pollutants

Material	Morphology/ Band gap (eV)	Light source	Pollutant	Experimental conditions			Photo degradation efficiency (%)	Synthesis method	Ref.
Bare				PC (g/L)	Pollutant (mg/L)*	Irradiation time			
BiOF	Steamed-rice-shaped 3.64	Four 4 W UV lamp	Phenol	1	0.25 mmol l^{-1}	75 min	>95	Precipitation	[109]
			Salicylic acid (SA)	1	5.0 mmol l^{-1}	75 min	>95		
			Methyl orange (MO)	1	20 mg l^{-1}	75 min	>95		
			Rhodamine B (RhB)	1	0.01 mmol l^{-1}	5 min	99		
BiOF	Nanosheets 3.93	UV light (λ>420 nm)	Rhodamine B (RhB)	z	10	60 min	79.3	Hydrothermal	[110]
Carbon Based									
BiOF/Bi_2O_3/rGO	Nanoparticles 1.12-1.18	500 W xenon lamp	Rhodamine B (RhB)	0.5	15	8 hrs	99	Hydrolysis	[111]
Ag-BiOF/g-C_3N_4	Square shaped	100 W halogen lamp	Methylene blue (MB)	1	7.5	6 hrs	78	Solvothermal	[112]

*Certain values mentioned in m mol

Table S5. Summary of literature on photocatalytic modified BiOX and BiOx/BiOY (X=Cl, Br, I; X≠Y) over various types of organic pollutants

Material	Morphology/ Band gap (eV)	Light source	Pollutant	Experimental conditions			Photo degradation efficiency (%)	Synthesis method	Ref.
				PC (g/L)	Pollutant (mg/L)*	Irradiation time			
x-BiOCl/y-BiOBr	Microspheres 2.89-2.26	300 W xenon lamp	Rhodamine B (RhB)	0.1	20	60 min	1 : 5=98	Microwave assisted co-precipitation	[113]
x% BiOI/BiOBr	Nanosheets 1.93-2.81	150 W tungsten halogen lamp	Methyl orange (MO)	Thin film	10	5 hrs	20%=40.8 40%=61.2 60%=51.1	Solvothermal	[114]
x% BiOCl/BiOI	Flower like 1.98-2.03	300 W xenon lamp	Methyl orange (MO)	0.5	10	20 min	20%=95	Hydrothermal	[115]
			Rhodamine B (RhB)	0.25	10	15 min	70%=98		
BiOBr/BiOI	Sheets 1.58-2.61	150 W xenon arc lamp	Crystal violet (CV)	—	10 ppm	48 hrs	99	Hydrothermal	[116]
x% BiOBr/BiOI	Microspheres 1.86-2.32	500 W xenon lamp	Rhodamine B (RhB)	0.4	15	40 min	50%=Complete degradation 90%=93.1	One pot solvothermal	[117]
			Tetracycline (TC)	0.4	40	50 min	10%=92.8 50%=83		

Table 5. Continued

Material	Morphology/ Band gap (eV)	Light source	Pollutant	Experimental conditions			Photo degradation efficiency (%)	Synthesis method	Ref.
				PC (g/L)	Pollutant (mg/L)*	Irradiation time			
x% BiOI/BiOCl	Nanosheets 1.97-2.93	1000 W xenon lamp	Bisphenol A (BPA)	1	20	60 min	90%=97.8	One pot solvothermal	[118]
BiOX (X=Cl, Br, I)	Nanoplates nanosheets BiOCl=3.20 BiOBrg=2.72 BiOI=1.76	300 W xenon arc lamp	Methyl orange (MO)	1	20	60 min 180 min	Microspheres=Complete degradation nanoplates=40	Solvothermal	[119]
BiOX (X=Cl, Br, I)	Nanoplates BiOCl=3.54 BiOBr=2.97 BiOI=1.98	UV LED, GLED, RLED, BLED	Rhodamine B (RhB)	1	1.08×10^{-5} M	120 min 240 min	BiOCl=100 (UV, BLED) BiOCl=71.1 (GLED), 70.1 (RLED) BiOBr=100 (UV, BLED) BiOI=67.6 (UV LED), 83.4 (RLED), 69.6 (BLED), 54.0 (GLED)	Hydrothermal	[120]
BiOX (X=Cl, Br)	Visible (λ>400 nm) BiOCl=3.29 BiOBr=2.76	500 W xenon lamp	Methyl orange (MO) Methylene blue (MB) Rhodamine B (RhB)	— — —	— — —	30 min 30 min 30 min	BiOBr=9.97 BiOBr=25.81 BiOBr=99.56 BiOCl=94.91 (λ>400 nm), 99.5 (λ>420 nm), 53.76 (λ>550 nm)	Chemical route	[121]
BiOX X (Cl, Br, I)	Flower like BiOCl=3.01-3.09 BiOBr=2.46-2.70 BiOI=1.46-1.63	500 W xenon lamp	Cr (VI) Rhodamine B (RhB)	1 0.1	60 1×10^{-5} mol/*l*	120 min 20 min	— BiOCl=50% BiOBr=50% BiOI=Complete degradation	Microwave irradiation method	[122]
BiOX X=(Cl, Br, I)	Sheet like BiOI=1.76 BiOBr=2.75 BiOCl=3.19	Xenon lamp irradiation	Sodium penta-chlorophenate (PCP-Na)	1.5	20 µL	60 min	BiOCl=95.9 BiOBr=35.2 BiOI=8.9	Facile method	[123]
BiOX (X=Cl, Br, I)	Flower shaped BiOCl=3.15 BiOBr=2.76 BiOI=1.80	800 W xenon lamp	Rhodamine B (RhB)	0.5	10	60 min	—	Solvothermal	[124]

Table 5. Continued

Material	Morphology/ Band gap (eV)	Light source	Pollutant	Experimental conditions			Photo degradation efficiency (%)	Synthesis method	Ref.
				PC (g/L)	Pollutant (mg/L)*	Irradiation time			
BiOX (X=Cl, Br, I)	Flower like BiOCl=2.84 BiOBr=2.60 BiOI=1.69	Visible light (λ>400 nm)	Rhodamine B (RhB)	—	—	40 min	BiOCl=97 BiOBr=100 BiOI=97	Facile method	[125]
Composite/heterostructure									
SiO_2/BiOX (X=Cl, Br, I)	BiOCl=3.2 BiOBr=2.75 BiOI=1.76	Iodine tungsten lamp	Rhodamine B (RhB)	Film	10	3 hrs	BiOBr=98	Sol-gel	[126]
Ag/AgX/BiOX (X=Cl, Br)	Nanoparticles — —	500 W xenon lamp	Rhodamine B (RhB)	0.2	10	60 min	—	Low-temperature chemical bath	[127]
(Rh, Pd, Pt)/BiOX (X=Cl, Br, I)	Nanoplates 1.71-2.81	150 W tungsten halogen lamp	Acid orange II	0.5	20	—	—	Chemical route	[128]
$CoFe_2O_4$/BiOX (X=Cl, Br, I)	Micro flowers BiOCl=3.2 BiOBr=2.8 BiOI=1.8	Visible light	Rhodamine B (RhB)	0.25	BiOCl=20 BiOBr=20 BiOI=40	6 hrs	>95%	Solvothermal	[129]
Carbon based									
g-C_3N_4/BiOX (X=Cl, Br, I)	Nanoplates —	500 W xenon lamp	Rhodamine B (RhB)	1	7	50 min	Complete degradation	Immersion-hydrolysis	[130]
BiOX/Carbon cloth	Nano sheet	300 W xenon lamp	Rhodamine B (RhB) 4-Nitrophenol (4-NP)	— —	10 20	120 min 120 min	BiOCl=96 BiOCl=98	Solvothermal	[131]
CNT's/BiOX (X=Cl, I)	Fibers 3.08	Sunlight simulator lamp	Methyl orange (MO)	0.1	20	80 min	—	Chemical route	[132]
Doped									
Europium- BiOX (X=Cl, Br, I)	Nanoflakes BiOCl=3.36 BiOBr=2.76 BiOI=1.67	150 W xenon lamp	Rhodamine B (RhB)	1	5×10^{-6} mol/*l*	BiOCl=20 min BiOBr=25 min BiOI=100 min	Complete degradation Complete degradation Complete degradation	Microwave synthesis	[133]

*Certain values mentioned in mol, M or ppm

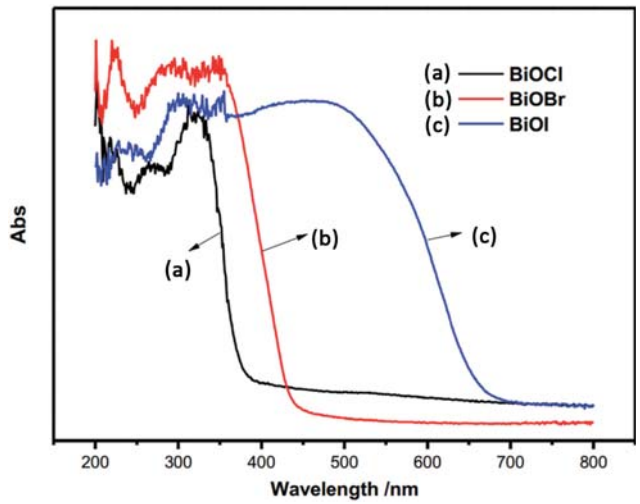

Fig. S1. UV absorption spectra for BiOCl, BiOBr and BiOI [reproduced with permission of Shen et al., Copyright 2015, RSC] [126].

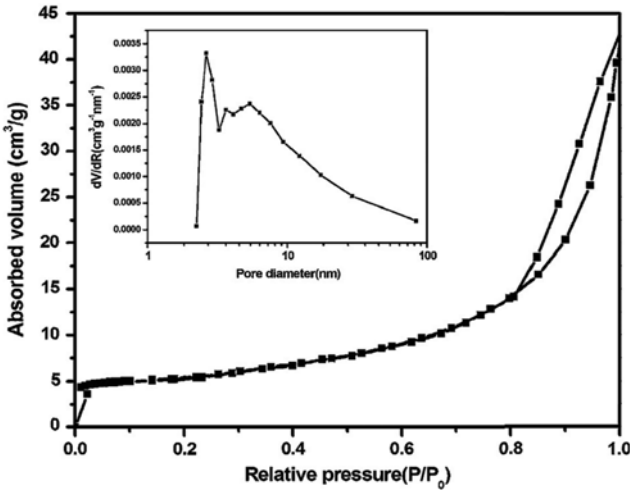

Fig. S2. N_2 adsorption-desorption isotherm and BJH pore size distribution (inset) of Fe doped BiOBr sample [reproduced with permission of Liu et al., Copyright 2012, Springer] [80].

MECHANISMS PROPOSED FOR PHOTOCATALYTICALLY ACTIVE BIOX

A. Heterojunction System

Heterojunction semiconductors are an effectual strategy that can be successfully applied to develop photocatalysts that responds to visible light for splitting of water. Heterojunctions formed between two/three solid state photocatalysts or p-n materials with matching band potential, aids in enhancing the separation efficiency of photo-produced electron-hole pairs [134]. The heterojunction formation depends on the ultimate position of CBM and VBM of both the materials in the composite. Based on the alignment of these energy levels, the heterostructures could be described in three ways (Fig. A). The high photocatalytic activity is a result of effective separation of electron and hole pairs and suppression of electron-hole recombination. In type I heterojunction, CB level of semiconductor B has higher energy than the CB level of semiconductor A while VB level of semiconductor B has lower energy than of semiconductor A. Under illumination, photoexcited electrons can transfer from CB (B) to CB (A), while the holes can be transferred from VB (B) to VB (A) when both materials are in sufficient contact. Thus, both electrons and holes get collected in semiconductor A resulting in their recombination which yields no improvement in photocatalytic activity. Type II structure with optimum band positions and have photogenerated electrons and holes spatially separated from each other leads to improved photocatalytic activity. Type III works similar to type II except only that the band positions are even further set off [135]. The increased photocatalytic activity of the p-type BiOCl and n-type $SrFe_{12}O_{19}$ composite as compared to the pure BiOCl was ascribed to the formation of the p-n type heterojunction between these two materials. Migration of photo-excited carriers is promoted by inner filed formation which thus facilitates the charge separation and enhances the overall performance [136].

B. Z-scheme

A Z-scheme junction is a special type of heterojunction (Fig. B). Inspired by natural photosynthesis process, Z-scheme is a two-step photoexcitation system wherein it involves two different semiconductors, each having a potential for either oxidation or reduction of water, together with shuttle redox mediator. Therefore, Z-scheme provides an advantage of using photocatalysts that are active only for half reactions of water splitting, in contrary to conventional one step photoexcitation system where both oxidation and reduction of water takes place at single-component photocatalyst which may

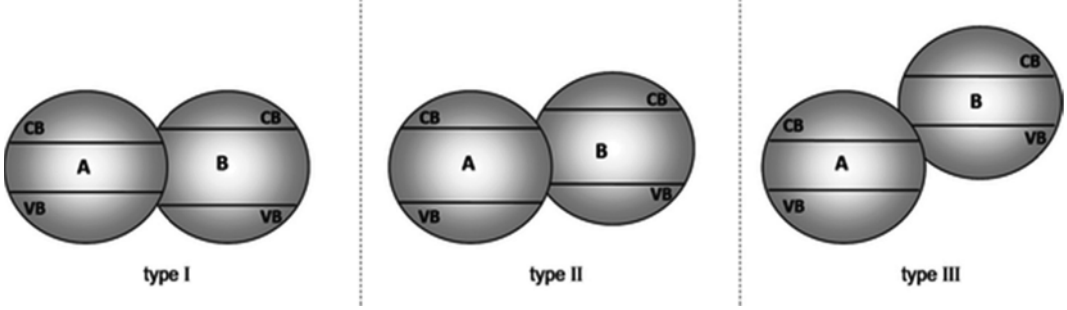

Fig. A. Different types of semiconductor hetrojunction (Reproduced with permission from Marschall et al., Copyright 2013, John Wiley and Sons).

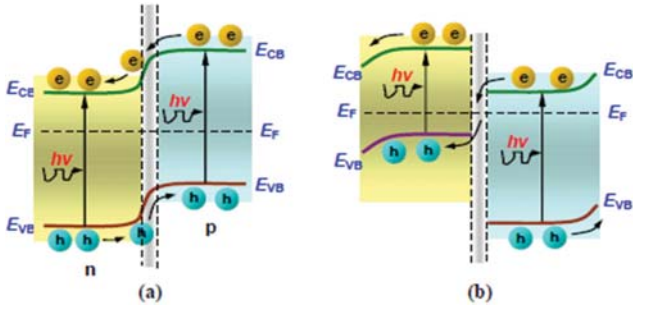

Fig. B. Schematic illustration of the energy band diagram showing migration of charge carriers in (a) common p-n heterostructure and (b) z-scheme heterostructure (Reproduced with permission from He et al., Copyright 2014, Elsevier).

not always be sufficient for high charge-separation efficiency [137]. Utilization efficiency of visible energy in Z-scheme is increased as amount of energy required for photoexcitation of electron-hole pair in each photocatalyst is reduced. Shuttle redox mediator is a reversible donor/acceptor ion which transfers the electrons from conduction band (CB) of one photocatalyst to valence band (VB) of other photocatalyst and similarly holes from VB of one to CB of other photocatalyst. Concentration of redox mediator and pH value are vital factors that decide photocatalytic activity [137]. Z-scheme is used for oxygen generation by water splitting and hydrogen production can also be achieved by use of suitable co-catalyst. Use of metal oxide semiconductors like rutile TiO_2, $BiVO_4$, WO_3, PtO_x, RuO_2, BiOX etc in Z-scheme are well reported for oxygen, hydrogen evolution and heterogenous photocatalysis [138-142]. The Z-scheme concept was nicely presented by Ohno et al., developed a photo electrochemical cell with Pt-TiO_2 particles suspended in cathode compartment using Bromide as electron donor and TiO_2 in anode chamber with Fe^{3+} ions as electron acceptors [143]. Hydrogen evolved from cathode and oxygen from anode compartment respectively. Reaction on each photocatalyst is as follows:

On Pt-TiO_2:
$2H^+ + 2e^- = H_2$
$2Br^- + 2h^+ = Br_2$

On TiO_2:
$Fe^{3+} + e^- = Fe^{2+}$
$2H_2O + 4h^+ = O_2 + 4H^+$

Bai et al. synthesised direct Z scheme BiOCl/g-C_3N_4 composite using one step chemical bath method with enhanced photocatalytic activity compared to pure counterparts [28]. Ye et al. developed Ag/AgX/BiOX (X=Cl, Br) composite photocatalyst and observed enhanced photocatalytic performance than Ag/AgX and BiOX alone [127]. Their study also revealed an interesting finding about the role of Ag in Ag/AgCl/BiOCl and Ag/AgBr/BiOBr which was different in both the cases. SPR effect was found dominant in case of Ag/AgBr/BiOBr whereas, enhanced activity in Ag/AgCl/BiOCl was possibly found due to Z-scheme bridge. Z-scheme provides huge potential and flexibility for the development of high efficient visible light driven photocatalysts with BiOX and other semiconductors.

REFERENCES

1. K. L. Zhang, C. M. Liu, F. Q. Huang, C. Zheng and W. D. Wang, *Appl. Catal., B: Environ.*, **68**, 125 (2006).
2. Q. Wang, J. Hui, Y. Huang, Y. Ding, Y. Cai, S. Yin, Z. Li and B. Su, *Mater. Sci. Semicond. Process.*, **17**, 87 (2014).
3. Z. Q. Shi, Y. Wang, C. M. Fan, Y. F. Wang and G. Y. Ding, *Trans. Nonferrous Met. Soc. China*, **21**, 2254 (2011).
4. X. Zhang, X. B. Wang, L. W. Wang, W. K. Wang, L. L. Long, W. W. Li and H. Q. Yu, *ACS Appl. Mater. Interfaces*, **6**, 7766 (2014).
5. Y. Wang, Z. Q. Shi, C. M. Fan, X. G. Hao, G. Y. Ding and Y. F. Wang, *Int. J. Miner. Metall. Mater.*, **19**, 467 (2012).
6. L.-P. Zhu, G.-H. Liao, N.-C. Bing, L.-L. Wang, Y. Yang and H.-Y. Xie, *Crystengcomm*, **12**, 3791 (2010).
7. K. Zhang, J. Liang, S. Wang, J. Liu, K. Ren, X. Zheng, H. Luo, Y. Peng, X. Zou, X. Bo, J. Li and X. Yu, *Cryst. Growth Des.*, **12**, 793 (2012).
8. M. Guan, C. Xiao, J. Zhang, S. Fan, R. An, Q. Cheng, J. Xie, M. Zhou, B. Ye and Y. Xie, *J. Am. Chem. Soc.*, **135**, 10411 (2013).
9. A. Tadjarodi, O. Akhavan and K. Bijanzad, *J. Nanostruct.*, **5**, 1 (2015).
10. D. Zhang, L. Chen, C. Xiao, J. Feng, L. Liao, Z. Wang and T. Wei, *J. Nanomater.*, **33**, 2016 (2016).
11. A. Tadjarodi, O. Akhavan, K. Bijanzad and M. M. Khiavi, *Monatshefte Für Chemie - Chem. Mon.*, **147**, 685 (2016).
12. Y. Zuo, C. Wang, Y. Sun and J. Cheng, *Mater. Lett.*, **139**, 149 (2015).
13. F. Duo, Y. Wang, X. Mao, X. Zhang, Y. Wang and C. Fan, *Appl. Surf. Sci.*, **340**, 35 (2015).
14. Y.-F. Li, M. Zhang, D.-L. Guo, F.-X. He, Y.-Z. Li and A.-J. Wang, *J. Nanomater.*, **2014**, 215 (2014).
15. C. Wang, F. Zhang, J. Cheng, Y. Cui and S. Wu, *ICMREE China*, 10 (2013).
16. B. Gao, A. K. Chakraborty, J. M. Yang and W. I. Lee, *Bull. Korean Chem. Soc.*, **31**, 1941 (2010).
17. L. Zhang, X. Yuan, H. Wang, X. Chen, Z. Wu, Y. Liu, S. Gu, Q. Jiang and G. Zeng, *RSC Adv.*, **5**, 98184 (2015).
18. B. C. Cao, P. Y. Dong, S. Cao and Y. H. Wang, *J. Am. Ceram. Soc.*, **96**, 544 (2013).
19. S. Shenawi-Khalil, V. Uvarov, E. Menes, I. Popov and Y. Sasson, *Appl. Catal., A: Gen.*, **413-414**, 1 (2012).
20. S. Shamaila, A. K. L. Sajjad, F. Chen and J. Zhang, *J. Colloid Interface Sci.*, **356**, 465 (2011).
21. L. Zhang, W. Wang, S. Sun, Y. Sun, E. Gao and J. Xu, *Appl. Catal., B: Environ.*, **132-133**, 315 (2013).
22. L. Shan, G. Wang, L. Liu and Z. Wu, *J. Mol. Catal. a-Chemical*, **406**, 145 (2015).
23. D. Yue, D. Chen, Z. Wang, H. Ding, R. Zong and Y. Zhu, *Phys. Chem. Chem. Phys.*, **16**, 26314 (2014).
24. V. J. Babu, R. S. R. Bhavatharini and S. Ramakrishna, *RSC Adv.*, **4**, 29957 (2014).
25. J. Hu, G. Xu, J. Wang, J. Lv, X. Zhang, T. Xie, Z. Zheng and Y. Wu, *Dalton Trans.*, **44**, 5386 (2015).
26. Z. He, Y. Shi, C. Gao, L. Wen, J. Chen and S. Song, *J. Phys. Chem. C*, **118**, 389 (2014).
27. W. Wang, M. He, H. Zhang and Y. Dai, *Int. J. Electrochem. Sc.*, **11**,

1831 (2016).
28. Y. Bai, P.-Q. Wang, J.-Y. Liu and X.-J. Liu, *RSC Adv.*, **4**, 19456 (2014).
29. H. Tang, Y. Ao, P. Wang and C. Wang, *Mater. Sci. Semicond. Process.*, **27**, 909 (2014).
30. M. Zhang, C. Shao, X. Zhang and Y. Liu, *CrystEngComm*, **17**, 7276 (2015).
31. F. Deng, X. Lu, F. Zhong, X. Pei, X. Luo, S. Luo, D. D. Dionysiou and C. Au, *Nanotechnology*, **27**, 65701 (2016).
32. S. Kang, R. C. Pawar, Y. Pyo, V. Khare and C. S. Lee, *J. Exp. Nanosci.*, **8080**, 1 (2015).
33. S. Zhang, D. Wang and L. Song, *Mater. Chem. Phys.*, **173**, 298 (2016).
34. M. Nussbaum, N. Shaham-Waldmann and Y. Paz, *J. Photochem. Photobiol. A Chem.*, **290**, 11 (2014).
35. F. Xie, X. Mao, C. Fan and Y. Wang, *Mater. Sci. Semicond. Process.*, **27**, 380 (2014).
36. G. Chen, G. Chen, Y. Wang, Q. Wang and Z. Zhang, *J. Nanomater.*, **2015**, 5 (2015).
37. Z. Kun, R. E. N. Kuaixia and Y. U. Xibin, *J. Shanghai Jiaotong Univ.*, **42**, 73 (2013).
38. M. Gao, D. Zhang, X. Pu, X. Shao, H. Li and D. Lv, *J. Am. Ceram. Soc.*, **99**, 881 (2015), DOI:10.1111/jace.14012.
39. J. Yu, B. Wei, L. Zhu, H. Gao, W. Sun and L. Xu, *Appl. Surf. Sci.*, **284**, 497 (2013).
40. G. K. Tripathi and R. Kurchania, *J. Mater. Sci. Mater. Electron.*, **27**, 5079 (2016).
41. K. Zhang, D. Zhang, J. Liu, K. Ren, H. Luo, Y. Peng, G. Li and X. Yu, *CrystEngComm*, **14**, 700 (2012).
42. Q. Wang, J. Hui, J. Li, Y. Cai, S. Yin, F. Wang and B. Su, *Appl. Surf. Sci.*, **283**, 577 (2013).
43. F. Chang, J. Luo, X. Wang, Y. Xie, B. Deng and X. Hu, *J. Colloid Interface Sci.*, **459**, 136 (2015).
44. C. Xue, J. Xia, T. Wang, S. Zhao, G. Yang, B. Yang, Y. Dai and G. Yang, *Mater. Lett.*, **133**, 274 (2014).
45. V. J. Babu, M. Sireesha, R. S. R. Bhavatharini and S. Ramakrishna, *Mater. Lett.*, **169**, 50 (2016).
46. Y. Feng, L. Li, J. Li, J. Wang and L. Liu, *J. Hazard. Mater.*, **192**, 538 (2011).
47. R. Li, C. Fan, X. Zhang, Y. Wang, Y. Wang and H. Zhang, *Thin Solid Films*, **562**, 506 (2014).
48. H. L. Chen, W. W. Lee, W. H. Chung, H. P. Lin, Y. J. Chen, Y. R. Jiang, W. Y. Lin and C. C. Chen, *J. Taiwan Inst. Chem. Eng.*, **45**, 1892 (2014).
49. M. Shang, W. Wang and L. Zhang, *J. Hazard. Mater.*, **167**, 803 (2009).
50. D. Zhang, M. Wen, B. Jiang, G. Li and J. C. Yu, *J. Hazard. Mater.*, **211-212**, 104 (2012).
51. J. Xu, W. Meng, Y. Zhang, L. Li and C. Guo, *Appl. Catal., B: Environ.*, **107**, 355 (2011).
52. Z. Jiang, F. Yang, G. Yang, L. Kong, M. O. Jones, T. Xiao and P. P. Edwards, *J. Photochem. Photobiol. A Chem.*, **212**, 8 (2010).
53. B. Chai, H. Zhou, F. Zhang, X. Liao and M. Ren, *Mater. Sci. Semicond. Process.*, **23**, 151 (2014).
54. W. Ling-Li, M. Wan-Hong, W. Shu-Lian, Z. Yu, J. Man-Ke, L. RuiPing, Z. Ai-Qing and H. Ying-Ping, *J. Nanomater.*, **2012**, 91 (2012).
55. H. Shu, K. Sun, H. Li, J. Xia, H. Xu, L. Xu, M. He and J. Di, *Micro Nano Lett.*, **8**, 450 (2013).
56. K. Bijanzad, A. Tadjarodi, O. Akhavan and M. M. Khiavi, *Res. Chem. Intermed.*, **42**, 2429 (2016).
57. J. Xia, J. Di, S. Yin, H. Li, L. Xu, Y. Xu, C. Zhang and H. Shu, *Ceram. Int.*, **40**, 4607 (2014).
58. J. Zhang, F. Shi, J. Lin, D. Chen, J. Gao, Z. Huang, X. Ding and C. Tang, *Chem. Mater.*, **20**, 2937 (2008).
59. X. J. Wang, X. N. Xu, Y. J. Han and X. N. Chen, *Cryst. Res. Technol.*, **50**, 405 (2015).
60. H. Zhang, Y. Yang, Z. Zhou, Y. Zhao and L. Liu, *J. Phys. Chem. C*, **118**, 14662 (2014).
61. Y. Huo, J. Zhang, M. Miao and Y. Jin, *Appl. Catal., B: Environ.*, **111-112**, 334 (2012).
62. Z. Liu, H. Ran, J. Niu, P. Feng and Y. Zhu, *J. Colloid Interface Sci.*, **431**, 187 (2014).
63. X.-X. Wei, H. Cui, S. Guo, L. Zhao and W. Li, *J. Hazard. Mater.*, **263**, 650 (2013).
64. W. Guo, Q. Qin, L. Geng, D. Wang, Y. Guo and Y. Yang, *J. Hazard. Mater.*, **308**, 374 (2016).
65. Y. Guo, H. Huang, Y. He, N. Tian, T. Zhang, P. K. Chu, Q. An and Y. Zhang, *Nanoscale*, **7**, 11702 (2015).
66. X. Meng, L. Jiang, W. Wang and Z. Zhang, *J. Photoenergy*, **2015**, 9 (2015).
67. G. L. Wang, M. X. Liu, G. S. Cao and Y. J. Bai, *Micro & Nano Lett.*, **10**, 115 (2015).
68. H. Lin, J. Cao, B. Luo, B. Xu and S. Chen, *Chinese Sci. Bull.*, **57**, 2901 (2012).
69. L. Kong, Z. Jiang, T. Xiao, L. Lu, M. O. Jones and P. P. Edwards, *Chem. Commun. (Camb).*, **47**, 5512 (2011).
70. W. Li, Y. Tian, P. Li, B. Zhang, H. Zhang, W. Geng and Q. Zhang, *RSC Adv.*, **5**, 48050 (2015).
71. X. Li, X. Mao, X. Zhang, Y. Wang, Y. Wang, H. Zhang, X. Hao and C. Fan, *Sci. China Chem.*, **58**, 457 (2015).
72. S. Shenawi-Khalil, V. Uvarov, S. Fronton, I. Popov and Y. Sasson, *J. Phys. Chem. C*, **116**, 11004 (2012).
73. Y. Li, Y. Liu, J. Wang, E. Uchaker, Q. Zhang, S. Sun, Y. Huang, J. Li and G. Cao, *J. Mater. Chem. A*, **1**, 7949 (2013).
74. G. Jiang, X. Li, Z. Wei, T. Jiang, X. Du and W. Chen, *Powder Technol.*, **260**, 84 (2014).
75. S. Janani, K. S. RS, P. Ellappan and L. R. Miranda, *J. Environ. Chem. Eng.*, **4**, 534 (2016).
76. Y. J. You, Y. X. Zhang, R. R. Li and C. H. Li, *Russ. J. Phys. Chem. A*, **88**, 2188 (2014).
77. J. Fu, Y. Tian, B. Chang, F. Xi and X. Dong, *J. Mater. Chem.*, **22**, 21159 (2012).
78. X. X. Wei, C. M. Chen, S. Q. Guo, F. Guo, X. M. Li, X. X. Wang, H. T. Cui, L. F. Zhao and W. Li, *J. Mater. Chem. A*, **2**, 4667 (2014).
79. R. Wang, G. Jiang, X. Wang, R. Hu, X. Xi, S. Bao, Y. Zhou, T. Tong, S. Wang, T. Wang and W. Chen, *Powder Technol.*, **228**, 258 (2012).
80. Z. Liu, B. Wu, Y. Zhu, D. Yin and L. Wang, *Catal. Lett.*, **142**, 1489 (2012).
81. G. Jiang, X. Wang, Z. Wei, X. Li, X. Xi, R. Hu, B. Tang, R. Wang, S. Wang, T. Wang and W. Chen, *J. Mater. Chem. A*, **1**, 2406 (2013).

82. C. Bi, J. Cao, H. Lin, Y. Wang and S. Chen, *RSC Adv.*, **6**, 15525 (2016).
83. G. H. Jiang, X. Li, Z. Wei, T. T. Jiang, X. X. Du and W. X. Chen, *Acta Metall. Sin. English Lett.*, **28**, 460 (2015).
84. X. Shi, X. Chen, X. Chen, S. Zhou, S. Lou, Y. Wang and L. Yuan, *Chem. Eng. J.*, **222**, 120 (2013).
85. S. Xie, K. Ouyang and X. Ma, *Ceram. Int.*, **40**, 12353 (2014).
86. C. Yu, C. Fan, J. C. Yu, W. Zhou and K. Yang, *Mater. Res. Bull.*, **46**, 140 (2011).
87. Y. Li, J. Wang, H. Yao, L. Dang and Z. Li, *J. Mol. Catal. A Chem.*, **334**, 116 (2011).
88. X. Chang, J. Huang, Q. Tan, M. Wang, G. Ji, S. Deng and G. Yu, *Catal. Commun.*, **10**, 1957 (2009).
89. Q. C. Liu, D. K. Ma, Y. Y. Hu, Y. W. Zeng and S. M. Huang, *ACS Appl. Mater. Interfaces*, **5**, 11927 (2013).
90. Y. Lei, G. Wang, S. Song, W. Fan, M. Pang, J. Tang and H. Zhang, *Dalton Trans.*, **39**, 3273 (2010).
91. J. Liu, H. Li, N. Du, S. Song and W. Hou, *RSC Adv.*, **4**, 31393 (2015).
92. X. Xiao and W.-D. Zhang, *J. Mater. Chem.*, **20**, 5866 (2010).
93. Y. Mi, M. Zhou, L. Wen, H. Zhao and Y. Lei, *Dalton Trans.*, **43**, 9549 (2014).
94. W. W. Lee, C. S. Lu, C. W. Chuang, Y. J. Chen, J. Y. Fu, C. W. Siao and C. C. Chen, *RSC Adv.*, **5**, 23450 (2015).
95. Y. Wang, K. Deng and L. Zhang, *J. Phys. Chem. C*, **115**, 14300 (2011).
96. Z. Liu, X. Xu, J. Fang, X. Zhu, J. Chu and B. Li, *Appl. Surf. Sci.*, **258**, 3771 (2012).
97. C. Liao, Z. Ma, G. Dong and J. Qiu, *Appl. Surf. Sci.*, **314**, 481 (2014).
98. H. Liu, W. Cao, Y. Su, Y. Wang and X. Wang, *Appl. Catal., B: Environ.*, **111-112**, 271 (2012).
99. Y. Liu, W. Yao, D. Liu, R. Zong, M. Zhang, X. Ma and Y. Zhu, *Appl. Catal., B: Environ.*, **163**, 547 (2015).
100. Y. Chen, X. Xu, J. Fang, G. Zhou, Z. Liu, S. Wu, W. Xu, J. Chu and X. Zhu, *Sci. World J.*, **2014**, 8 (2014).
101. C. Liu, J. Wang, X. Wang, F. Li, L. Zhang and Y. Chen, *Russ. J. Phys. Chem. A*, **89**, 2313 (2015).
102. L. Chen, D. Jiang, T. He, Z. Wu and M. Chen, *CrystEngComm*, **15**, 7556 (2013).
103. J. Di, J. Xia, M. Ji, L. Xu, S. Yin, Q. Zhang, Z. Chen and H. Li, *Carbon N. Y.*, **98**, 613 (2016).
104. H. Liu, W. R. Cao, Y. Su, Z. Chen and Y. Wang, *J. Colloid Interface Sci.*, **398**, 161 (2013).
105. R. He, S. Cao, D. Guo, B. Cheng, S. Wageh, A. A. Al-Ghamdi and J. Yu, *Ceram. Int.*, **41**, 3511 (2015).
106. J. Di, J. Xia, M. Ji, B. Wang, S. Yin, H. Xu, Z. Chen and H. Li, *Langmuir*, **32**, 2075 (2016).
107. Y. Chen, Q. Lu, X. Yan, Q. Mo, Y. Chen, B. Liu, L. Teng, W. Xiao, L. Ge and Q. Wang, *Nanoscale Res. Lett.*, **11**, 60 (2016).
108. N. Ekthammathat, S. Kidarn, A. Phuruangrat, S. Thongtem and T. Thongtem, *Res. Chem. Intermed.*, **42**, 5559 (2015).
109. W. Su, J. Wang, Y. Huang, W. Wang, L. Wu, X. Wang and P. Liu, *Scr. Mater.*, **62**, 345 (2010).
110. S. Zou, F. Teng, C. Chang, Z. Liu and S. Wang, *RSC Adv.*, **5**, 88936 (2015).
111. L. Hu, S. Dong, Q. Li, J. Feng, Y. Pi, M. Liu, J. Sun and J. Sun, *J. Alloys Compd.*, **633**, 256 (2015).
112. S. Vadivel, V. P. Kamalakannan, N. P. Kavitha, T. Santhoshini Priya and N. Balasubramanian, *Mater. Sci. Semicond. Process.*, **41**, 59 (2016).
113. S. Zhang and J. Yang, *Colloids Surf. A Physicochem. Eng. Asp.*, **420**, 89 (2015).
114. Z. Liu, H. Ran, B. Wu, P. Feng and Y. Zhu, *Colloids Surf. A Physicochem. Eng. Asp.*, **452**, 109 (2014).
115. T. B. Li, G. Chen, C. Zhou, Z. Y. Shen, R. C. Jin and J. X. Sun, *Dalton Trans.*, **40**, 6751 (2011).
116. Y. R. Jiang, S. Y. Chou, J. L. Chang, S. T. Huang, H. P. Lin and C. C. Chen, *RSC Adv.*, **5**, 30851 (2015).
117. L. Lin, M. Huang, L. Long, Z. Sun, W. Zheng and D. Chen, *Ceram. Int.*, **40**, 11493 (2014).
118. X. Xiao, R. Hao, M. Liang, X. Zuo, J. Nan, L. Li and W. Zhang, *J. Hazard. Mater.*, **233-234**, 122 (2012).
119. X. Qin, H. Cheng, W. Wang, B. Huang, X. Zhang and Y. Dai, *Mater. Lett.*, **100**, 285 (2013).
120. K. Natarajan, H. C. Bajaj and R. J. Tayade, *J. Ind. Eng. Chem.*, **34**, 146 (2016).
121. X. Chang, M. A. Gondal, A. A. Al-Saadi, M. A. Ali, H. Shen, Q. Zhou, J. Zhang, M. Du, Y. Liu and G. Ji, *J. Colloid Interface Sci.*, **377**, 291 (2012).
122. G. Li, F. Qin, R. Wang, S. Xiao, H. Sun and R. Chen, *J. Colloid Interface Sci.*, **409**, 43 (2013).
123. X. Chang, J. Huang, C. Cheng, Q. Sui, W. Sha, G. Ji, S. Deng and G. Yu, *Catal. Commun.*, **11**, 460 (2010).
124. J. Xu, L. Li, C. Guo and Y. Zhang, 5th Int. Conf. Bioinforma. Biomed. Eng. iCBBE 2011, 3 (2011).
125. L. Chen, R. Huang, M. Xiong, Q. Yuan, J. He, J. Jia, M. Y. Yao, S. L. Luo, C. T. Au and S. F. Yin, *Inorg. Chem.*, **52**, 11118 (2013).
126. F. Shen, L. Zhou, J. Shi, M. Xing and J. Zhang, *RSC Adv.*, **5**, 4918 (2015).
127. L. Ye, J. Liu, C. Gong, L. Tian, T. Peng and L. Zan, *ACS Catal.*, **2**, 1677 (2012).
128. C. Yu, F. Cao, G. Li, R. Wei, J. C. Yu, R. Jin, Q. Fan and C. Wang, *Sep. Purif. Technol.*, **120**, 110 (2013).
129. Y. I. Choi, Y.-I. Kim, D. W. Cho, J.-S. Kang, K. T. Leung and Y. Sohn, *RSC Adv.*, **5**, 79624 (2015).
130. J. Sun, J. Song, M. A. Gondal, S. Shi, Z. Lu, Q. Xu, X. Chang, D. Xiang and K. Shen, *Res. Chem. Intermed.*, **41**, 6941 (2014).
131. L. Li, M. Zhang, Y. Liu and X. Zhang, *Nano*, **10**, 73 (2015).
132. B. Weng, F. Xu and J. Xu, *J. Nanopart. Res.*, **16**, 2766 (2014).
133. A. Dash, S. Sarkar, V. N. K. B. Adusumalli and V. Mahalingam, *Langmuir*, **30**, 1401 (2014).
134. S. Y. Chai, Y. J. Kim, M. H. Jung, A. K. Chakraborty, D. Jung and W. I. Lee, *J. Catal.*, **262**, 144 (2009).
135. R. Marschall, *Adv. Funct. Mater.*, **24**, 2421 (2014).
136. T. Xie, L. Xu, C. Liu, J. Yang and M. Wang, *Dalt. Trans.*, **43**, 2211 (2014).
137. K. Maeda, *ACS Catal.*, **3**, 1486 (2013).
138. R. Abe, K. Sayama, K. Domen and H. Arakawa, *Chem. Phys. Lett.*, **344**, 339 (2001).
139. M. Higashi, R. Abe, A. Ishikawa, T. Takata, B. Ohtani and K. Domen, *Chem. Lett.*, **37**, 138 (2008).

140. H. Kato, M. Hori, R. Konta, Y. Shimodaira and A. Kudo, *Chem. Lett*., **33**, 1348 (2004).
141. K. Sayama, R. Yoshida, H. Kusama, K. Okabe, Y. Abe and H. Arakawa, *Chem. Phys. Lett*., **277**, 387 (1997).
142. K. Sayama, K. Mukasa, R. Abe, Y. Abe and H. Arakawa, *Chem. Commun*., **23**, 2416 (2001).
143. T. Ohno, S. Saito, K. Fujihara and M. Matsumura, *Bull. Chem. Soc. Jpn*., **69**, 3059 (1996).